UNIVERSITÀ DEGLI STUDI DI NAPOLI FEDERICO II

FACOLTÀ DI SCIENZE MATEMATICHE FISICHE E NATURALI

DOTTORATO IN SCIENZE CHIMICHE
XXIV CICLO 2008 – 2011

Polyolefins based hybrid nanocomposites

Tutore: **Candidato:**
Prof. Claudio De Rosa   *Marilena Pezzuto*

Cotutore
Dott.ssa Clara Silvestre

Relatore:
Prof. Finizia Auriemma

Coordinatore:
Prof. Lucio Previtera

Be the Best of Whatever You Are

If you can't be a pine on the top of the hill,
Be a scrub in the valley but be
The best little scrub by the side of the rill;
Be a bush if you can't be a tree.

If you can't be a bush be a bit of the grass,
And some highway happier make;
If you can't be a muskie then just be a bass
But the liveliest bass in the lake!

We can't all be captains, we've got to be crew,
There's something for all of us here,
There's big work to do, and there's lesser to do,
And the task you must do is the near.

If you can't be a highway then just be a trail,
If you can't be the sun be a star;
It isn't by size that you win or you fail
Be the best of whatever you are!

Douglas Malloch (1877 - 1938)

Summary

Introduction

In recent years, Polymer Layered Silicate nanocomposites PLSn have attracted great interest, both in industry and in academia, because they often exhibit remarkable improvement in properties when compared with virgin polymer or conventional micro and macro-composite. These improvements can include higher moduli, [1-5] increased strength and heat resistance, [6] decreased gas permeability [7-11] and flammability [12] and increased biodegradability rate of biodegradable polymers.[13]

The properties of the nanocomposites depend not only on the kind of constituents and composition, but mainly on the degree of dispersion of nanoscale particles inside the matrix. The very large interfacial area and the nanoscopic dimension of the particles lead to the formation of hybrid structures which fundamentally differentiates polymer nanocomposites from traditional filled plastic.[14-15]

1. Layered Silicate

The common used layered silicate for the preparation of PLSn belongs to the-family of 2:1 layered or phyllosilicates. Their crystal structure consists of layers made up of two tetrahedral coordinated silicon atoms fused to an edge-shared octahedral sheet of their aluminium or magnesium hydroxide. The layer thickness is around 1 nm, and the lateral dimensions of these layers may vary from 30nm to several microns or larger, depending on the particular layered silicate. Stacking of the layers leads to a regular *van der Waals* gap between the layers called *the interlayer or gallery*. Isomorphic substitution within the layer (for example, Al^{3+} replaced by Mg^{2+} or Fe^{2+}, or Mg^{2+} replaced by Li^{1+}) generates negative charges that are counterbalanced by alkali and alkaline earth cations situated inside the galleries. This type of layered silicate is characterized by a moderate surface charge known as the cation exchange capacity (CEC), and is generally expressed as mequiv/100 gm. The value of this charge is an average over the whole crystal as it varies from layer to layer. Montmorillonite (MMT), hectorite, and saponite are the most commonly used layered silicate.

In the case of tetrahedrally substituted layered silicates the negative charge is located on the surface of silicate layers, and hence, the polymer matrices can react interact more readily with these than with octahedrally-substituted material.
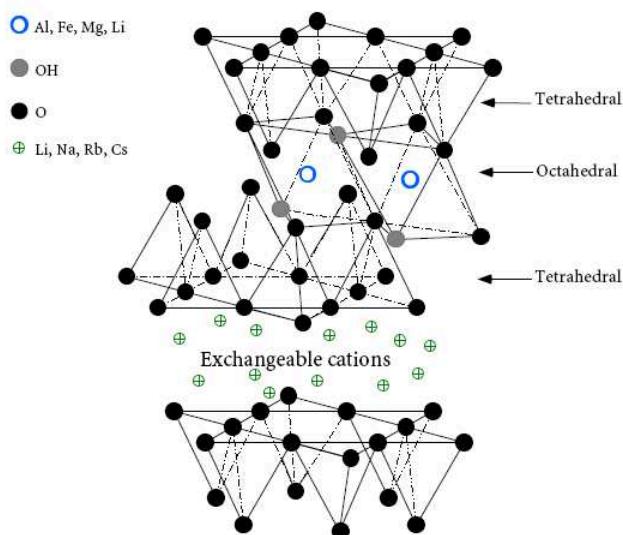
Figura 1: structure of 2:1 phyllosilicates

2. Structure and Properties of organically modified layered silicate (OMLS)

The physical mixture of a polymer and layered silicate may not form a nanocomposite. Because of their large surface energy, clay platelets tend to stick together particularly when dispersed in non polar polymer environment. Agglomeration of clay platelets leads to tactoid structures with reduced aspect ratio and reduced properties efficiency. This situation is similar to polymer blends and, in most cases, separation into discrete phases takes place. In immiscible systems, which typically correspond to the more conventionally filled polymers, the poor physical interaction between the organic and the inorganic components leads to poor mechanical and thermal properties. In contrast, strong interaction between the polymer and the layered silicate in PLSn lead to a dispersion of the clay particles at the nanometer level. As a result, nanocomposites exhibit unique properties not shared by their micro counterparts or conventionally filled polymers.[1-5]

Pristine layered silicates usually contain hydrated Na^+ or K^+ ions. [16] In this pristine state, layered silicate are only miscible with hydrophilic polymers, such as poly(ethylene oxide) (PEO), [17] or poly(vinyl alcohol) (PVA). [18] A route to render layered silicates miscible with non polar polymer matrices consists in converting the normally hydrophilic silicate surface to an organophilic one, making possible the intercalation of many engineering polymer. Generally, this can be done by ion-exchange reactions with cationic surfactants including primary, secondary, tertiary, and quaternary alkylammonium or alkylphosphonium cations. Alkylammoniun or alkylphosphonium cations in the organosilicates lower the surface energy of the inorganic host, improve the wetting characteristics of the polymer

matrix and finally result in a larger interlayer spacing. Additionally, the alkylammonium or alkylphosphonium cations can provide functional groups that can react with the polymer matrix, or in some cases initiate the polymerization of monomers to improve the interfacial adhesion between the inorganic and the polymer matrix . [19]

3. Morphology of polymer layered silicate

A few weight percent of layered silicates-properly dispersed throughout the polymer matrix creates much higher surface area for polymer/filler interaction as compared to conventional composites. Depending on the strength of interfacial interaction between the polymer matrix and layered silicate (modify or not), three different types of PLSn nanocomposites are thermodynamically achievable (figure 2): intercalated, exfoliated and flocculated that present an intermediated morphology. [20]

Their appearance is dependent on the strength of interfacial interaction between the polymer matrix and the filler. A reported by Ray and Okamoto in intercalated nanocomposites, [21] the insertion of a polymer matrix into the layered silicate structure occurs in a crystallographically regular fashion, regardless of the clay to polymer ratio. Intercaleted nanocomposites are normally interlayer by a few molecular layers of the polymer. In some cases silicate layers are flocculated due to hydroxylated edge-edge interaction of the silicate layers. The exfoliated nanocomposiste consist of individual nanometre-thick layers suspended in a polymer matrix and are a result of extensive penetration of the polymer in the silicate layer. The d-spacing between the silicate layers is significantly expanded up to 10 nm or more. Exfoliation has been the ultimate goal of most researchers in this area because this morphology is expected to lead to dramatics improvements of the properties with a reduce loading of fillers compared to traditional composites.
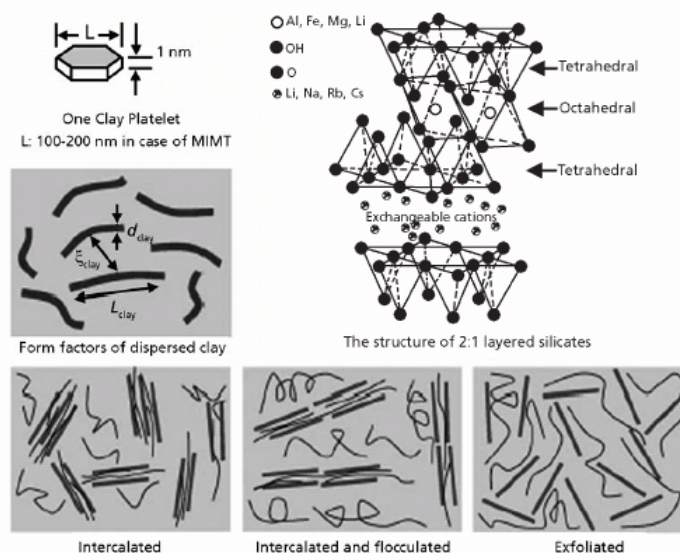
Figura 2: schematically illustration of three different typers od thermodynamically achievable polymer/layered silicate nanocomposites.

The overall morphology in nanocomposites in very complex and the classification given above for discerning the degree of intercalation is too simplified. In the range of exfoliated structures, and additional classification (into ordered, partially ordered and disordered structures) was introduce to adequately describe nanoscale morphologies and to avoid confusion in the structure-properties relationship of nanocomposites. Vaia [22] proposed an expanded classification scheme where the intercalated and exfoliated structure can be listed into ordered and disordered structures, depending on the change spacing and orientation of nanoparticles. An intermediate morphology between intercalation and exfoliation called partial exfoliation, can also be present. In the case of ordered exfoliation the ordered and parallel arrangement of nanolayers is preserved and a homogenous morphology is observed. In the case of disordered exfoliation, individual nanolayers are randomly distributed in the matrix.

The overall morphology in clay nanocomposites is still more complex as changes in the structure and morphology of the matrix can also occur due to the presence of the fillers. Consequently the characterization of the structures for both polymer matrix and layer structure dispersion of nano and microscales is essential to establish relationship among preparation, morphology processing and properties.

4. Preparative methods of Polymer nanocomposites.

Intercalation of the polymers in layered hosts, such as layered silicates must be pursued to obtain PLSn with high properties efficiency. The preparative methods are divided into three main groups according to the starting materials and processing techniques: intercalation of polymer or pre-polymer from solution, in situ intercalative polymerization method and melt intercalation method.

4.1 Intercalation of polymer or pre-polymer from solution

The solution dispersion method involves mixing a preformed polymer solution with the clay. This is based on a solvent systems in which the polymer or pre polymer is soluble and the silicate layers are swellable. The layered silicate is first swollen in a solvent, such as water, chloroform, or toluene. When the polymer and layered silicate solution are mixed, the polymer chain intercalate and displace the solvent within the interlayer of the silicate. Upon solvent removal, the intercalated structure remains, resulting in PLSn. In this method the nature of the solvent is critical in facilitating the insertion of the polymer between the silicate layer, polarity of the medium is being a determining factor for intercalation. [23]

For the overall process in which polymers is exchange with the previously intercalated solvent in the gallery, a negative variation of Gibbs free energy is required. The driving force for the polymer intercalation into layered silicate from solution is the entropy gained by desorption of solvent molecules which compensates for the decrease entropy of the confined intercalated chains.[24] To achieve this goal either the polymer must be polar enough to have positive interaction energy with the surface of the clay must be organically modified.

Polymer typically used in solution dispersion are polyethylene oxide (PEO), [17] polyvinyl alcohol (PVA), [18] polyimide (PI), [25] or polyurethanes (PU), [26] polyamide (PA) and high density polyethylene with suface modify. [27]

This method is applicable for certain polymer solvent pairs and useful for intercalation of the polymer with little or not polarity; it facilities production of thin films with intercalated and oriented clay layers. However from commercial point of view this methods involves copious use of organic solvent which may be hazardous to personnel and the environment witch renders it economically prohibitive.

4.2 *In situ intercalative polymerization method*

In situ polymerization involves the dispersion and distribution of the clay layers in the monomer flowed by polymerization. The layered silicate is swollen within the liquid monomer or a monomer solution so the polymer formation can occur between the intercalated sheets. Polymerization can be initiated either by heat, or radiation, by diffusion of a suitable initiator, or by an inorganic initiator or catalyst fixed through cation exchange inside the interlayer before the swelling step.

This technique has been known for long time. [23] However, in situ polymerization technique gained considerable momentum since the report of synthesis of a Nylon-6/MMT nanocomposite by the Toyota research group, [28] where very small amounts of layered silicate loading resulted in pronounced improvements in thermal and mechanical properties.

Usuki et al. first reported the ability of ω-amino acid ($NH_2(CH_2)_{n-1}COOH$ (where n=2,3,4,5,6,8,11,12,18) modified Na^+-MMT to be swollen by the ε-caprolactam monomer at 100°C and subsequently initiating its ring opening polymerization to obtain Nylon 6 MMT nanocomposites.[29] For the intercalation of ε-caprolactam, they chose the ammonium cation ω-amino acids, because these acids catalyze ring-opening polymerization of ε-caprolactam. The number of carbon atoms in α ω-amino acids has a strong effect on the swelling behaviour. The figure 3 represents the conceptual view of the swelling behaviour of ω-amino acid modified Na^+-MMT by ε-caprolactam.
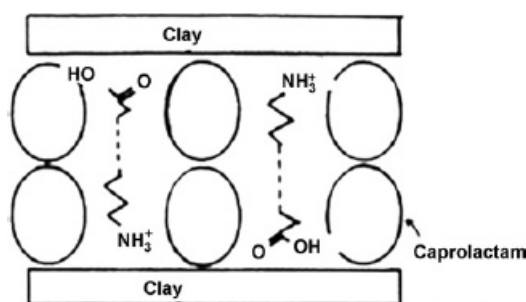
**Figure 3: Swelling behaviour of ω-amino acid modified Na^+-MMT by ε-caprolactam.**

4.3 Melt intercalation method

This technique consists of blending the layered silicate with the polymer matrix in the molten state. Under such conditions if the layer surfaces are sufficiently compatible with the chosen polymer the polymer can crawl into the interlayer space and form either an intercalated or an exfoliated nanocomposite.[30] This method has great advantages over either in situ intercalative polymerization or polymer solution intercalation. First, this method is environmentally benigh due to the absence of organic solvent, Second, it is compatible with current industrial process, such as extrusion and injection molding. The melt intercalation methods allows the use of polymers which were previously not suitable for in situ polymerization or solution intercalation.

Figure 4 represents a schematic illustration of nanocomposites formation by direct melt intercalation in modified galleries
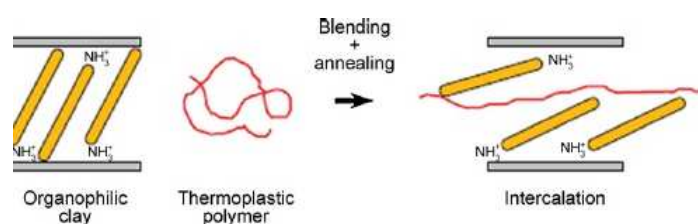
Figure 4: a schematic illustration of nanocomposites formation by direct melt intercalation in modified galleries

A range of nanocomposites with structure from intercalated to exfoliated can be obtained, depending on the degree of penetration of the polymer chains into the silicate galleries So far, experimental indicate that the outcome of polymer intercalation depends critically on silicate functionalization and constituent interactions. *Sinha Rai and Okamoto* [21] observed that:

(a) an optimal interlayer structure on the modified clay with respect to the number per unit area and size of surfanctant chain, is most favourable for nanocomposite formation, and

(b) polymer intercalation depends on the existence of polar interactions between modified clay and the polymer matrix.

Based on the *Vaia et al.*,[24] general guidelines may be established for selecting potentially compatible polymer/OMLS systems. Polymer containing polar groups are capable of

associative interactions, such as Lewis-acid/Lewis-base interactions or hydrogen bonding, thus leading to intercalation. The polarizability or hidrophilicity of the polymer also depends on the size of the functional group, as shorter functional groups lead to improved hydrophilicity in order to minimize unfavourable interactions between the aliphatic chains and the polymer.

To overcome this difficulty *Usuky et al.* [31] first reported a novel approach to prepare PP/nanocomposites using a functional oligomer (PP-OH) with polar telechelic OH groups as a compatibilizer. In this approach, PP-OH was intercalated between the layers of $2C_{18}$-MMT, and then it was melt mixed with PP to obtain the nanocomposite with intercalaeted structure. *Kawasaki et al* [32] reported the preparation of PP/nanocomposite obtained by melt blending of iPP, a maleic anhydride grafted PP oligomer (PP-g-MA), and clays modified with stearylammonium using a twin-screw extruder. This study using two different types of maleic anhydride modified PP oligomer with different amounts of maleic anhydride groups and two types of organically modified clays to understand the miscibility effect of the oligomers on the disperdibility of the OMLS in the PP matrix. In addition they also studied the effect of hybridation on the mechanical properties when compared with neat PP and PP/nanocomposites without oligomers. WAXD analyses and TEM observations established the intercalated structure for all nanocomposites, On the basis of WAXD patterns and TEM images, they proposed a possible mechanism of dispersion of intercalated clay layers in the PP matrix. Figure 5 shows a schematic presentation of the mixing process of the three components, i.e., PP, PP-g-MA, and OMLS into the nanocomposites, It is believed that the driving force of the intercalation originates from the maleic anhydride group and to oxygen groups of the silicate through hydrogen bonding.
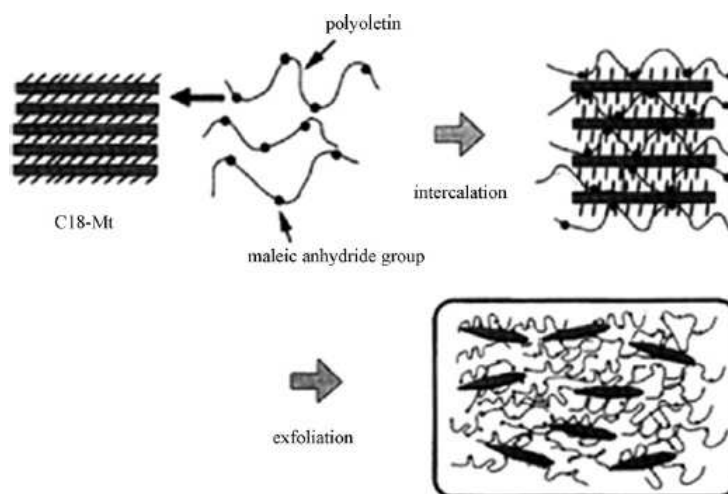
Figure 5: Schematic representation of the dispersion process of the OMLS in the polymer matrix with the aid of PP-MA

5. PP/nanocomposites

Polymers with high barrier properties are currently in great demand, especially in packaging industry, where they are replacing many traditional materials. However, in comparison with traditional containers (glass, metal, and paper), plastic packages are more permeable to gases, water vapour, and aroma compounds. In food packaging, where long shelf life is required, often they fail by allowing oxygen and water vapour to migrate through the wall, ruining the properties of the food product.[33]

Recently, hybrid inorganic–organic materials, in which reinforcing material are truly dispersed on a nanoscale level in a polymeric matrix, have attracted attention as alternative route to improve polymer barrier properties.

In the field of packaging isotactic polypropylene (iPP) films holds a prominent position in because of their transparency, brilliance, low specific weight, chemical inertness and good processability. Unfortunately, polypropylene, like other polyolefins, is characterized by low barrier properties, which results in poor protection of the packaged food.[34] One of the most useful methods to improve polypropylene drawbacks is to add a second component, to use multilayers films, etc.[35-38] Isotropic films of isotactic polypropylene iPP/ hydrogenated oligocyclopentadiene (HOCP) blends were introduced a few years ago in the packaging. It was found that for given conditions of preparation (melting temperature and rate of cooling) the films presented reduced permeability to oxygen and to aroma, together with increase of elastic modulus and optical properties, compared with that of the pure iPP film.

HOCP is an amorphous resin with glass transition much higher that the Tg of iPP. HOCP is a mixture of cis and trans isomers hydrogenated after oligomerization. HOCP is a commercial resin provided by Exxon mobil chemical with low molecular weight (M_w=680) and T_g of 89°C with trade name **Escorez** (ESC).

HOCP is available to use in the food packaging because it has good heat stability and barrier properties, transparency and good twist-wrap properties. The systems iPP/HOCP was soon studied by several investigators and various papers have been published concerning the blends [39-41] and the commercial isotropic film. [42] The results indicate that iPP and HOCP were completely miscible in the melt. After solidification the samples, were constituted by one amorphous phase (formed by amorphous iPP and HOCP) and, depending on the cooling process from the melt and on thickness of the sample, by iPP molecules crystallized in monoclinic α form or assuming the smectic modification. Then it was found by *Cimmino et*

al. [43] that this systems was not completely miscible in the melt but in a certain range of the temperature and composition a phase separation of the amorphous was found. In fact it was detected the existence of both upper and lower cloud point curves (ucp-curve and lcp-curve). Figure 6 shows the phase diagram of iPP/HOCP systems showing both UCST is the lower critical solution temperature and LCST is the upper critical solution temperature.
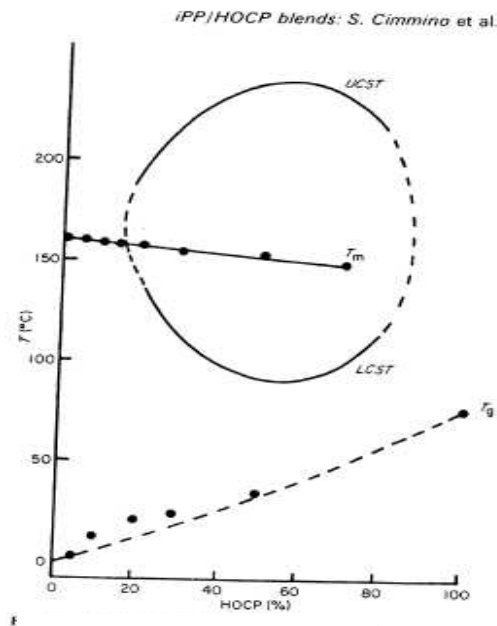
Figure 6: the phase diagram of iPP/HOCP (Escorez) systems

Escorez is a commercial hydrocarbon cycloalifatic resin provided by Exxon Mobil Chemical with low molecular weight (M_w=680) and T_g of 89°C

6. Goal of Thesis

The goal of this research is twofold:

1. to complete the study of the properties of iPP modified with Escorez resin;

2. to improve these properties by making nanocomposites with the addition of of clay for potential use in the packaging sector. In particular two kind of clays were used: unmodified clay (dellite HPS) and modify clay (Dellite 67G) both provided by Laviosa Chimica Mineraia.

The study of the structure, morphology and thermal, rheological, mechanical and barrier properties of the binary and ternary system will be reported as function of composition, kind of constituents and preparation conditions .

Moreover for all the systems the study on crystallization in situ under shear and during cooling will be reported. These crystallization studies have drawn much interest in recent years, because it implies the possibility of controlling and predicting the final morphologies and properties of semi-crystalline polymers in current transformation processes, like injection molding or extrusion where due to flow and non isothermal conditions both nucleation and growth are very different from those encountered under quiescent isothermal conditions.[44-46]

References

(1) Giannelis, E.P. *Adv.Mater*. **1996**, 8, 29.

(2) Giannelis, E.P.,; Krishnamoorti, R.; Manias, E. *Adv. Polym Sci*. **1999**, 138, 107.

(3) LeBaron, P.C,; Wang, Z.; Pinnavaia, T.J. *Appl. Clay Sci*. **1999**, 15, 11

(4) Vaia, R.A.;Price, G.; Ruth,P.N.; Nguyen, H.T.;Lichtenhan,*J. Appl. Clay Sci*.**1999**,15, 67.

(5) Biswas, M.; Sinha Ray, S. *Adv. Polym. Sci*. **2001**, 155, 167.

(6) Giannelis, E.P. *Appl. Organomet. Chem*. **1998**, 12, 675.

(7) Xu, R.; Manias, E.; Snyder, A.J.; Runt, J. *Macromolecules* **2001,** 34, 337.

(8) Bharadwaj, R.K. *Macromolecules* **2001**,34, 1989.

(9) Messersmith, P.B.; Giannelis, E.P. *J. Polym. Sci., Part A: Polym. Chem.* **1995**, 33, 1047

(10) Yano. K.; Usuki, A.;, Okada, A.; Kurauchi, T.; Kamigaito, O. *J. Polym. Sci. Part A: Polym. Chem*. **1993**, 31, 2493.

(11) Kojima, Y.; Usuki, A.; Kawasumi, M.; Fukushima, Y.; Okada, A.; Kurauchi, T.; Kamigaito, O. *J. Mater. Res*. **1993**, 8, 1179.

(12) Gilman, J.W.; Jackson, C.L.; Morgan, A.B.; Harris, Jr R.; Manias, E.; Giannelis,E.P.; Wuthenow, M.; Hilton, D.; Phillips, S.H. *Chem. Mater.* **2000**,12,1866.

(13) Sinha Ray, S.; Yamada, K.; Okamoto, M.; Ueda, K. *Nano Lett.* **2002**, 2, 1093.

(14)Novak, B.M. *Advanced Materials* **1993**, 5, 422.

(15) Messersmith, P.B. and Giannelis, E.P. *Chemistry of materials* **1994**, 6, 1719.

(16) Brindly,S.W.; Brown, G. editors. *Crystal structure of clay minerals and their X-ray diffraction.* London: Mineralogical Society; **1980**.

(17) Aranda, P.;Ruiz-Hitzky, E. *Chem. Mater*. **1992**, 4, 1395.

(18) Greenland, D.J. *J. Colloid. Sci.* **1963**,18, 647.

(19) Krishnamoorti, Vaia, R.A.; Giannelis, E.P. *Chem Mater* **1996**,8, 1728.

(20) Sinha Ray,S.; Okamoto, K.and Okamoto, M. *Macromolecules* **2001**, 34,12, 3819.

(21) Sinha Ray,S. and Okamoto, M. *Progress in Polymer Science* **2003**, 28, 1539.

(22) Vaia, R.A.; Jandt, K.; Kramer, E. and Giannelis,E. P. *Macromolecules,* **1995,**28 8080

(23) Theng, B.K.G., *Formation and properties of clay-polymer complexes*.Amsterdam/Oxford/New York, **1979** Elsevier Scientific Publishing Company. p .362.

(24) Vaia, R.A.; Giannelis, E.P. *Macromolecules* **1997**, 30, 7990.

(25) Yano, K.; Usuki,A.; Okada, A.; Kuraucki, T.; Kamigaito, O. *J. Polym. Sci. Part A: Polym. Chem.***1993***,* 31, 2493

(26) Xu, G.C.; Li, A.Y.; Zhang, L.D.; Wu, G.S.;. Yuan X.Y. and Xie, T.; *Journal of Applied Polymer Science* **2003**, 90, 837.

(27) Jeon, H.G.; Jung, H.T.; Lee, S.W.; Hudson, S.D. *Polym. Bull.* **1998**, 41, 107.

(28) Okada, A.;, Kawasumi, M.; Usuki, A.; Kojima, Y.; Kurauchi, T.; Kamigaito, O. In: Schaefer, D.W. and Mark,J.E. editors. *Polymer based molecular composites.* MRS Symposium Proceedings, Pittsburgh, vol. 171; **1990**, 45.

(29) Usuki, A.; Kawasumi, M.; Kojima, Y.; Okada, A.; Kurauchi, T.; Kamigaito, O. *J. Mater. Res.* **1993**, 8, 1174.

(30) Alexandre, M.; Dubois, P. *Mater. Sci. Eng. R* **2000**, 28, 1

(31) Usuki, A.; Kato, M.; Okada, A.; Kurauchi, T. *J Appl Polym Sci* **1997**, 63, 137.

(32) Kawasumi, M.; Hasegawa, N.; Kato, M.; Usuki, A.; Okada, A. *Macromolecules* **1997**,30, 6333.

(33) Lange, J.; Wyser, Y. *Packag Technol Sci* **2003**, 16, 149

(34) Karian, H.G. (ed.). *Handbook of Polypropylene and Polypropylene Composites*. Marcel Dekker: New York, **1999**.

(35). Karger-Kocsis J. (ed.). *Polypropylene: Structure, Blends and Composites*. Chapman and Hall: London, 1995.

(36). Deanin, R.D.; Manion, M.A. In *Handbook of Polyolefins*, Vasile C (ed.), 2nd edn. Marcel Dekker: New York, **2000**; 575.

(37). Avella, M.; Laurienzo, P.; Malinconico, M.; Martuscelli, E.; Volpe, M.G. In *Handbook of Polyolefins*, Vasile C (ed.), 2nd edn. Marcel Dekker: New York, **2000**; 723.

(38) Silvestre,C.; Duraccio,D.; Cimmino,S. *Progress in Polymer Science* **2011**, *36*, 1766

(39) Martuscelli, E.; Silvestre, C.; Canetti,M.; De Lalla, C.; A.Bonfanti and A. Seves, *Makromol. Chem.* **1989**, 190, 2615.

(40) Martuscelli, E.; Canetti,M. and A. Seves, *Polymer* **1989,** 30,304.

(41) Di Liello, V.; Martuscelli, E.; Ragosta, G. and Buzio, P. *J.Mater. Sci.*, **1989**,24,3232.

(42) Cimmino, S.; Guarrata, P.; Martuscelli,E. and Silvestre, C. *Polymer*, **1993**, 34, 972.

(43) Cimmino, S.; Di Pace, E.; Karasz, F.E.; Martuscelli,E. and Silvestre, C. *Polymer* **1993**, 34, 972.

(44) Keller, A.; Kolnaar, H.W.H in *Processing of Polymers*, edited by Cahn, R.W.; Haasen, P.; Kramer, E.J. Vol. 18, edited by H.E.H. Meijer (Wiley-VCH, **1997**) p. 189.

(45) Hill, M.J.; Keller, A. J. *Macromol. Sci. B*, **1969**, 3, 153

(46) Bashir, G.C.;. Odell,J.A.; Keller, A. *J. Mater. Sci.*, **1986,** 21, 3993

Chapter 1

Experimental Part

1.1 Materials

The isotactic polypropylene (iPP) is a commercial product, Moplen S30S (kindly provided by Basell, Ferrara, Italy) with a melt flow index of 1.8 g/10min and with molecular weight Mw= $2.7 \ 10^5$.

Escorez 5340, provided by Exxon Mobile Chemical Europe with molecular weight Mw= 680 g/mol and glass transition (T_g) of 89°C is hydrogenated mixture of isomers of cyclopentadiene. From now through the thesis it will be reported as Escorez.

The clays used are Dellite HPS and Dellite 67G, kindly supplied by Laviosa Chimica Mineraria SpA, Italy. Dellite HPS is a naturally occurring purified montmorillonite, Dellite 67G is Dellite HPS modified with a high content of quaternary ammonium salt (dimethyl dehydrogenated tallow ammonium). From now through the thesis they will be reported as HPS and 67G, respectively.

1.2 Sample Preparation

The hybrid systems were prepared by melt mixing in a Brabender-like apparatus at 210°C and 40 rpm for 10 minutes.

It is chosen to use two quantity of Escorez, 5 and 30% in weight of the blend iPP/Escorez. The amount of clay added to the blend was fixed to be 1g for every 100g of iPP/Escorez. The clay producing company indicates two methods to incorporate the clay in thermoset and thermoplastic systems; i) adding directly the clay to the compound; ii) adding up to 50% of clay in a master batch and then diluting the material in the final compound. For our purpose we have chosen the first method: the direct clay addition to the compound. The compositions of the systems are summarised in Table 1.

Slabs were prepared by compression molding in a press at 210°C for 3 minutes without applied pressure to allow complete melting and for other 3 minutes with the pressure raised to 10000 pounds. Then the plates of the press, fitted with cooling coils, were rapidly cooled to room temperature by using cold water. Finally the pressure was released and the mold, with a rectangular shape 1x 70 x 110 mm, removed from the press.

Films with thickness ≈ 130 μm for the determination of permeability to oxygen are prepared in the same condition of slabs.

Table 1: compositions of the systems prepared by melt mixing

Sample	iPP(%wt)	Escorez (%wt)	HPS pph[a]	67G pph[a]
iPP	100	-	-	-
iPP/HPS	99	-	1	-
iPP/67G	99	-	-	1
iPP/Esc/HPS	95	5	1	-
iPP/Esc/67G	95	5	-	1
iPP/Esc/HPS	70	30	1	-
iPP/Esc/67G	70	30	-	1
iPP/Esc	95	5	-	-
iPP/Esc	70	30	-	-

[a] **pph Part (or grams) per hundred parts (or grams) of iPP+Escorez**

1.3 Thermal analysis

The calorimetric properties of the compression-moulded blends were investigated with a differential scanning calorimeter (Mettler DSC822). The apparatus was calibrated with pure indium at various scanning rates. About 7 mg of the sample encapsulated in aluminium pans, was heated from -80°C to 200°C at a rate of 10°C/min (1st Run), kept at this temperature for 5 minutes and then cooled to -80°C at rate of 20°C/min; finally the sample was heated from -80 to 200°C at a rate of 10°C/min (2nd Run). All measurements were carried out in nitrogen atmosphere. The melting temperature (T_m) was obtained from the minimum of the endothermic peaks and the glass transition temperature (T_g) at the minimum of the peak obtained by applying the first derivative procedure. The crystallinity index, x_c, was calculated dividing the fusion entalphy for the theoretical value of 209 J/g of the melt enthalpy of 100% crystalline polypropylene.[1]

For non-isothermal melt crystallization, the raw sample was heated first to 210 °C and kept for 5 min in the cell to destroy any nuclei that might act as seed crystals. Then the sample was

cooled at constant rates of 5 10, 20 °C/min. The exothermic crystallization peak was recorded as a function of temperature.

1.4 Thermogravimetric analysis

The thermal stability of samples was conducted by using a Pyris diamond TG/DTA Perkin Elmer instrument at a scan rate of 20°C/min from 25 to 800°C in air and nitrogen atmosphere. Two recordings were performed for each sample.

1.5 Tensile mechanical test

Dumb-bell-shaped specimens (type IV according to ASTM D638) were cut from the slab using a steel punch cutter. Stress-strain curves were obtained by using an Instron machine (Model 4505) at room temperature (ca. 21-25°C) at a crosshead speed of 5 mm/min (ASTM D638). Young's modulus, stress and strain at yield and at break points were calculated from such curves on an average of 12 specimens.

1.6 Permeability Test

Permeability to oxygen was tested on films, by means of an ExtraSolution Multiperm apparatus. The instrumental apparatus consists of a double chamber diffusion cell. The film was inserted between the two chambers: a nitrogen flux containing oxygen enters in the lower one, and a dry nitrogen flux flows in the upper one. The partial pressure between the two chambers consents the oxygen trough the membrane that consists the sample. A zirconium oxide sensor measures the oxygen diffusion across the film. The exposed area of the film was 50 cm^2. Collected data were converted in oxygen transmission rate (OTR), that is, the time rate of oxygen flow between two parallel surfaces under steady conditions and specific temperature and relative humidity. Measurements were carried out in triplicate at 23°C and 0% RH. Oxygen permeability was calculated from OTR data by means of the equation (1):

$$\text{Permeability} = (\text{OTR} \cdot \text{thickness})/\Delta P \qquad (\text{Eq.1})$$

Where ΔP is the partial pressure between the two chambers of the instrument.

1.7 Structural and morphological analysis

1.7.1 Wide angle X-ray diffraction (WAXD) was carried out by using a Philips diffractometer with Cu Kα radiation (1.542Å) filtered by nickel. The profiles were recorded with a continuum scan of the Bragg angle 2 θ in the angular range of 2-45° with a step scan procedure, at room temperature with scan rate of 0.02°C/min.

An estimation of the crystallinity index, x_c, of the samples was obtained from the X-ray powder The indices of crystallinity (x_c) were evaluated from the X-ray powder diffraction profiles by the ratio between the crystalline diffraction area (A_c) and the total area of the diffraction profile (A_t), $xc=A_c/A_t$. The crystalline diffraction area has been obtained from the total area of the diffraction profile by subtracting the amorphous halo. The amorphous halo has been obtained from the X-ray diffraction profile of an atactic polypropylene.

1.7.2 Small-angle X-ray scattering (SAXS) data of compression-molded films were collected using a Kratky compact camera "SAXSess" (Anton Paar KG, Graz, Austria) in the slit collimation configuration, attached to a conventional X-ray source (Cu Kα, wavelength λ =1.5418 Å). The scattered radiation was recorded on a BAS-MS imaging plate (Fujifilm) and processed with a digital imaging reader (Fuji BAS 1800). The range of scattering vectors 0.06 nm^{-1} $\leq q \leq$ 5 nm^{-1}, where $q = (4\pi \sin \theta/\lambda)$ and 2θ is the scattering angle, was analyzed. After subtraction for dark current, the empty sample holder, and a constant background due to thermal density fluctuations, the slit smeared data were deconvoluted with the primary beam intensity distribution using the SAXSquant 2.0 software to obtain the corresponding pinhole scattering (desmeared) intensity distribution.

1.7.3 TEM analysis

All compression molded samples were ultramicrotomed with Reichert Ultracut E Ultramicrotome at room temperature with a diamond knife to give sections with a nominal thickness of 80 nm using a cutting speed of 2mm/sec at Center for Advanced Materials (CfAM, Reading University, UK). The sections were transferred from water (room temperature) to copper grids.

For the HPS and 67G powders, a small amount of clays were dispersed in Ethanol. After stirring to ensure a good dispersion of particles, a droplet of the suspension is placed on the copper grid and the solved evaporated.

Bright-field TEM images of all samples were obtained at 120 kV with FEI Tecnai G2 Spirit TWIN at Institute of Chemistry and Technology of Polymers (ICTP-CNR, Pozzuoli, Italy). The electron source consists of small crystal of lanthanum hexaboride (LaB_6).

The samples were analysed by taking several images of various magnifications over two to three sections per grid to ensure that analysis was based on a representative region of the sample.

1.7.4 SEM analysis

The surface analysis was performed by using a scanning electron microscope (SEM), model PHILIPS XL20, on cryogenically fractured surfaces of composites. Before the observation, samples were coated with an Au/Pd alloy by a SEM Coating unit E5 150.

1.8 Rheological measurements

The rheological measurements were performed in a Thermo Scientific Haake Reostress 6000 , using parallel plate-plate geometry. The disk-shaped samples with diameter of 2 cm and a thickness of 1.0 cm was prepared by compression molding in the same conditions of the slabs preparation (see paragraph sample preparation). The steady shear viscosity (η) respect to shear rates ($\mathring{y}$) was recorded . $\mathring{y}$ is controlled from a remote programmable controller, and it can be continuously varied to give shear rates between 0.01 s^{-1} and 10 s^{-1}. In the parallel plate instrument, two plates with the diameter of 2.5 cm and the gap size of 0.5 mm were used. All the measurements were performed at different temperatures (T = 165, 170, 175, 180, 185, 190°C).

1.9. Crystallization under shear

Crystallization under shear was studied using time-resolving in-situ small-angle X-ray scattering. SAXS measurements were carried out at the SAXS synchrotron beamline at "European Syncrotron radiation facility" (SRF) Grenoble, France, beamline 16 (syncrhrotron wavelength = 0.4795 Å).

In-situ small-angle X-ray scattering (SAXS) procedures to characterise the structures which develop during shearing and the crystallisation which takes place on cooling using a specially designed parallel-plate shear-flow system in conjunction with the intense x-ray beams available at a synchrotron radiation source. The shear stage was placed perpendicular to the

incident X-ray beam. Two dimensional scattering patterns were obtained by means a MarCCD 165 X-ray detector with resolution 2048*2048 pixels.

Essentially the sample is held between two thin mica discs supported on slotted plates within a small oven equipped with electrical heaters and a refrigerated gas cooling system. [4] This temperature control system provided defined heating rates up to 20ºC/min and cooling rates up to 10°C/min. This flow system allows X-ray and neutron scattering experiments to be performed during and following controlled shear flow. The incident X-ray beam lies normal to the plane of the sample and to the flow direction. The sample was placed at a distance of 6 m from detector.

The slots in the metal plates allowed the x-ray beam to pass through the sample for ~ 85% of a revolution. Collimation and masks prior to the rotating plate in the beam line were used to minimise the parasitic scattering from the spokes of the rotating plate as they cut the incident beam. An intelligent motor control system ensured that when the rotation was stopped, this took place at a rotation angle where the beam was not obscured by a metal spoke.

The parallel plate system means that the shear rate varies linearly across the radius. The small beam size is< 1mm means that the spread of shears probed by the x-ray beam is < 5%. Ex-situ experiments can benefit from the range of shear rates imposed on the sample by selecting different regions to probe.

Pre-moulded samples 1mm in thickness and 19 mm is diameter were used in these experiments. The measurement apparatus are shown in figure 1 and 2.

All polymer samples were subjected to the following thermal history: the samples were heated to 210°C and held for 10 min, then the melt was cooled at 10°C/min to room temperature. For each temperature (T_{shear}=165,170,175,180,185,190°C) a step shear of 100 s was applied. The shear rate was fixed at $10s^{-1}$. The thermal program used is shown in figure 3.

SAXS images were collected continuously, before, during and after cessation of the applied shear. The data acquisition time for each scattering pattern (image) was 3 s, with a pause time of 5 s between adjacent images. It should be noted that the scattering images represent the average of the scattered intensity from the scatterers across the thickness of the sample.
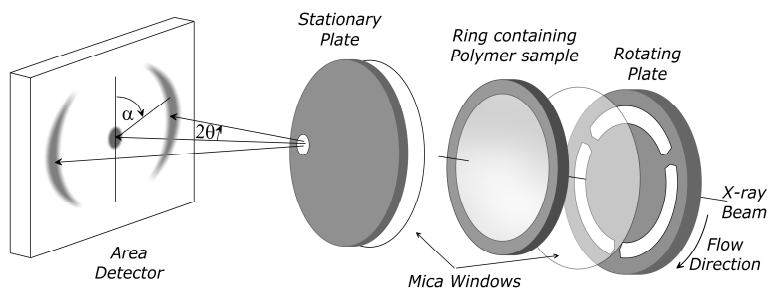
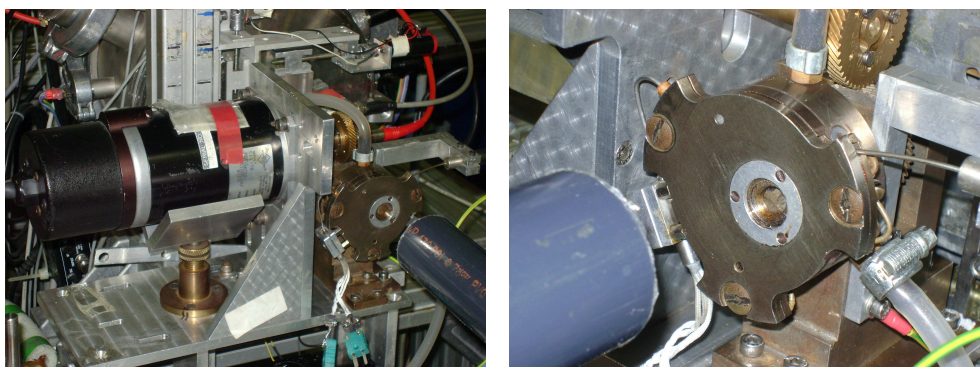**Figure 1 Schematic of parallel plate shear cell**

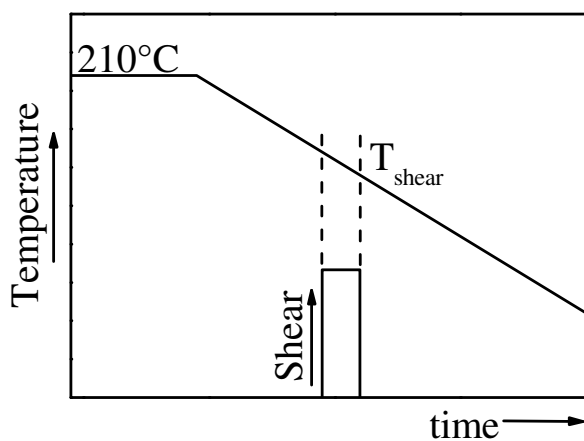**Figure 2. Apparatus for In-situ SAXS experiments**

Figure 3. Schematics of the temperature and shear conditions as a function of time during In-situ SAXS experiments

Some experiments were performed using a Couette style cell (figure 4) using the same basic shear cell but replacing the parallel plates by a rotating plate containing a ring and the fixed plate containing a cylinder. The gap between the ring and the cylinder was 1mm. In such an

arrangement the scattering vector lies in the plane containing the flow direction and the velocity gradient. In the schematic shown the velocity Ω_1 equals zero, is the cylinder is stationary. The beam was positioned to be in the centre of the gap.

Fixed plate and the rotating plate were covered with thin mica discs supported on metal plates with the same situation as in the parallel plate system that the beam could pass for 85% of the time.
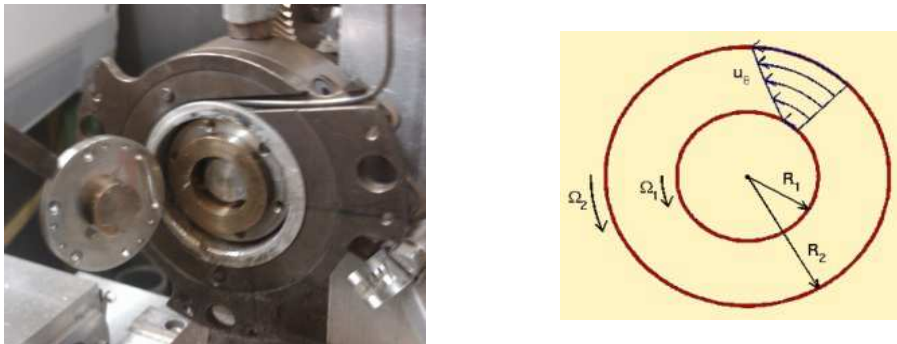
Figure 4: Zoom of Couette style cell and scheme of scattering vector in the plane containing the flow direction and the velocity gradient.

 The length of the Couette cell was 5mm. Throughout the sample volume the shear rate will be constant. There will be however, small end effects where the mica windows impose a second shear field. This will be small compared to that imposed by the ring and cylinder.

This arrangement was very convenient as the cell could be switched between the two modes of operation by changing the places, all factors such as the temperature profile etc remaining constant. The sample was moulded in the form of a cylindrical cell using the die shown in figure 5

Figure 5: cylindrical cell and the die

Each frame of the SAXS data was used to obtain quantitative structural information including orientation and crystallinity The crystallization kinetics have been analysed by calculating the invariant Ω (equation 2)

$$\Omega = \int_{0}^{\pi/2} \int_{Q=0}^{Q_{max}} |\underline{Q}|^2 \, I(|\underline{Q}|, \alpha) \, \sin \alpha \, dQ d\alpha \quad \text{Eq. 2}$$

The orientation parameter *<P2>* (equation 3) describes the preferential orientation of the crystal lamellae using the scattering which arises from these stacks of lamellae. Eq. 3

$$<P_2>_Q = \frac{1}{P_2^m} \int_{0}^{\pi/2} \frac{I(|\underline{Q}|, \alpha) \sin \alpha P_2(\cos \alpha) d\alpha}{I(|\underline{Q}|, \alpha) \sin \alpha d\alpha}$$

References

(1) Wunderlich, B. "*Macromolecular Physics*". New York: Academic Press, **1976**, Vol.2, 132.

(2). Aggarwal, S.L in *"Polymer Handbook"*, 2nd ed., Brandup, J.; Immergut, E.H., EDS., J.Wiley & Sons, New York **1975**, V-24.

(3) Roe, R.-J. *Methods of X-ray and Neutron Scattering in Polymer Science*; Oxford University Press: New York, **2000**.

(4) Nogales, A.; Thornley, S. A.; Mitchell, G. R. *J Macromol Sci- Physics* **2004**, B43, 1161.

Chapter 2

Morphological analysis (WAXD, SEM and TEM)

2.1 WAXD analysis

Figure 1 reports the WAXD profiles of compression molded iPP, iPP/clay, iPP/ESC and iPP/ESC/Clay blends and the profiles of Escorez, 67G and HPS as received by the companies. It is recalled that iPP can present several crystalline forms, as α, β, γ and a mesomorphic form.[1,2] The presence of the α -form is revealed by the peak between 2θ = 18–19° in the diffraction pattern, corresponding to the (130) plane, β -form is detectable by the peak at 15.5–16.5°, corresponding to the (200) β plane whereas γ-form is detectable by the peak at 20° corresponding to the (117) plane. The α form is that generally present in iPP obtained from cooling or quenching from the melt. The γ phase is obtainable for high MW by crystallization at elevated pressure. Figure 1(A) shows that the only form present in iPP, iPP/Clay, iPP/ESC and iPP/ESC/Clay samples is the monoclinic α-form. Figure 1(B) shows the diffractogram of Escorez with the typical shape of an amorphous material. The WAXD profile of 67G, Figure 1(C), presents three peaks at 2.6° (d = 3.4 nm), 4.7° (d =1.9 nm), and 7.2°(d =1.2 nm) corresponding to the (001), (002), and (003) plane respectively, indicating a multilayer structure. The peak at 7.2° is generated by the pristine MMT interlayer distance, whereas the two peaks at 2.6 and 4.7° indicate a bimodal modification due to the expansion of interlayer distance generated by the intercalation between the layers of dimethyl dehydrogenated tallow ammonium. The WAXD profile of HPS, Figure 1(D), shows a peak at 6.9° (d =1.3 nm) corresponding to the (001) plane and a spike at 8.8° indicating a uniform layer structure. [3]

The analysis of the diffraction patterns of the blends containing clays at low 2θ values (between 2 and 10°) can give information about the possible occurrence of intercalation and exfoliation. On thespectra of iPP/HPS and iPP/ESC5%/HPS and iPP/ESC30%/HPS (figure $1A_2$ and zoom at low value of 2θ), it is evident the reflection at 2θ = 6.9° which is the same value of the plain HPS, as it is shown in Figure 1 C; the Escorez does not induce any intercalation of HPS.

Passing to the analysis of the binary and ternary systems containing 67G (figure 1 A_3) only one defined peak is present at $2\theta \approx 6.5°$, whereas the plain 67G presents three peaks at 2θ =2.6° , 4.7° and 7.2°. The disappearance of the peak at 2θ = 2.6° corresponding to the (001) plane, does not means that the systems is intercalated. XRD results can be misinterpreted for

24

intercalated and immiscible polymer layered silicate nanocomposites that show peaks by XRD due to sampling problems, orientation, and poor calibration of most XRD instruments at very low angles. [4]

The analysis by SAXS at 1 <q<4 (see chapter 3) has shown, in all the blends containing 67G, a broad peak centered at $q \approx 1.9$ nm^{-1}. The (001) plane peaks of 67G in the same position of the SAXS profile of pure powder 67G indicates that the iPP does not intercalate into 67G layers.

In table 1 it is reported the crystallization index (x_c) calculated by WAXS refered to the blend. The presence of clays does not modify the crystallinity of iPP, and x_c decreases according to the amount of Escorez in the blends.

Table1. Crystallization index x_c calculated by WAXS, for iPP, iPP/Clay, iPP/ESC and iPP/ESC/Clay blends.

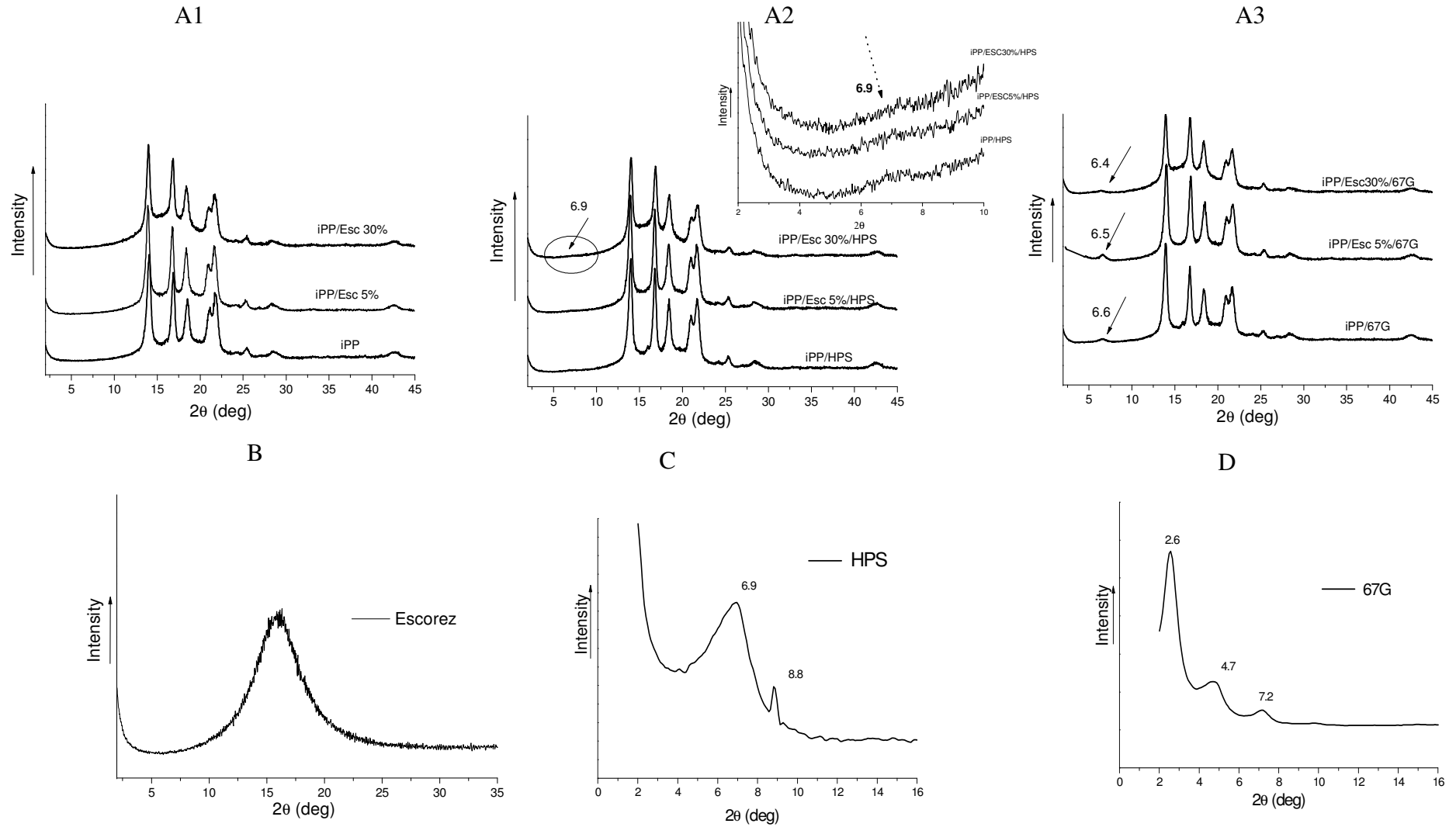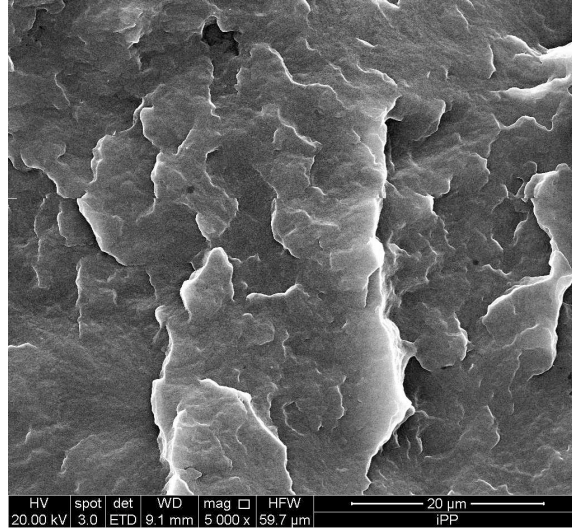| Sample	x_c (WAXS)
iPP	67
iPP/HPS	66
iPP/67G	67
iPP/ESC5%	61
iPP/ESC 30%	54
iPP/ESC5%/HPS	60
iPP/ESC5%/67G	61
iPP/ESC30%/HPS	54
iPP/ESC30%/67G	55

Figure 1: iPP, iPP/Clay, iPP/ESC and iPP/ESC/Clay blends in the compression molded sample(A$_1$, A$_2$, A$_3$); Escorez (B);HPS (C); 67G (D)
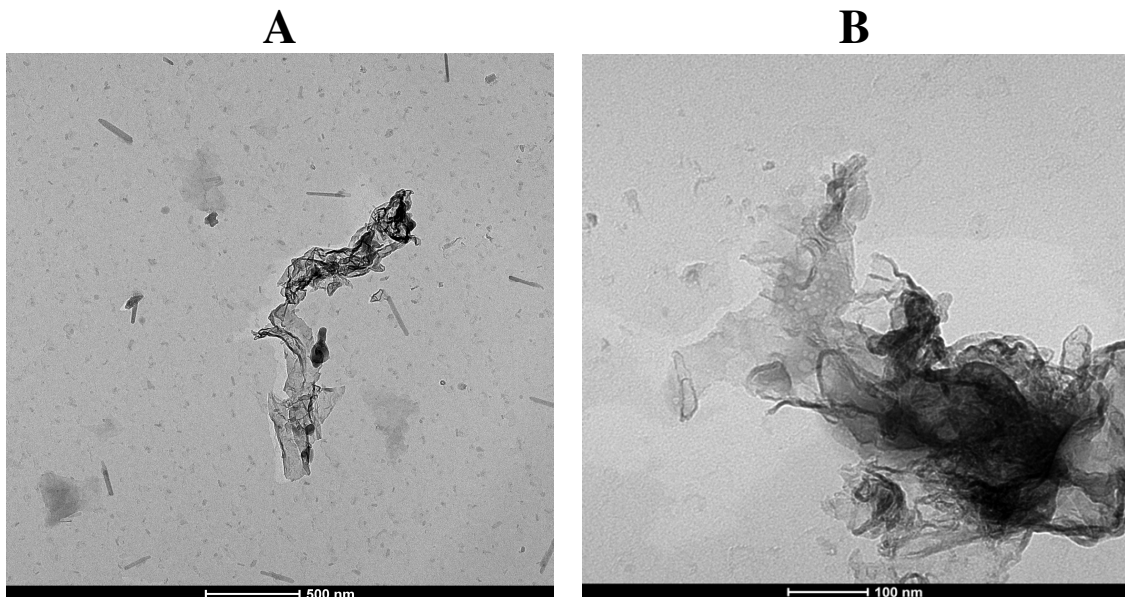
2.2 SEM and TEM analysis

Figure 1 shows the homogenous fractured surfaces of pure iPP at 5000x.

Figure 1: SEM micrograph (at 5000x) of fractured surface of pure iPP

Figures 2 A and B show TEM images of 67G and HPS respectively. The samples were prepared as described in experimental part chapter 1.


Figure 2: 67G (A) and HPS (B) powder

SEM and TEM micrographs of iPP/67G are shown in figure 3 A, B and C. The figures indicate a good dispersion of the clay 67G in the matrix (see comparison with figure 2 A).

A

B

C
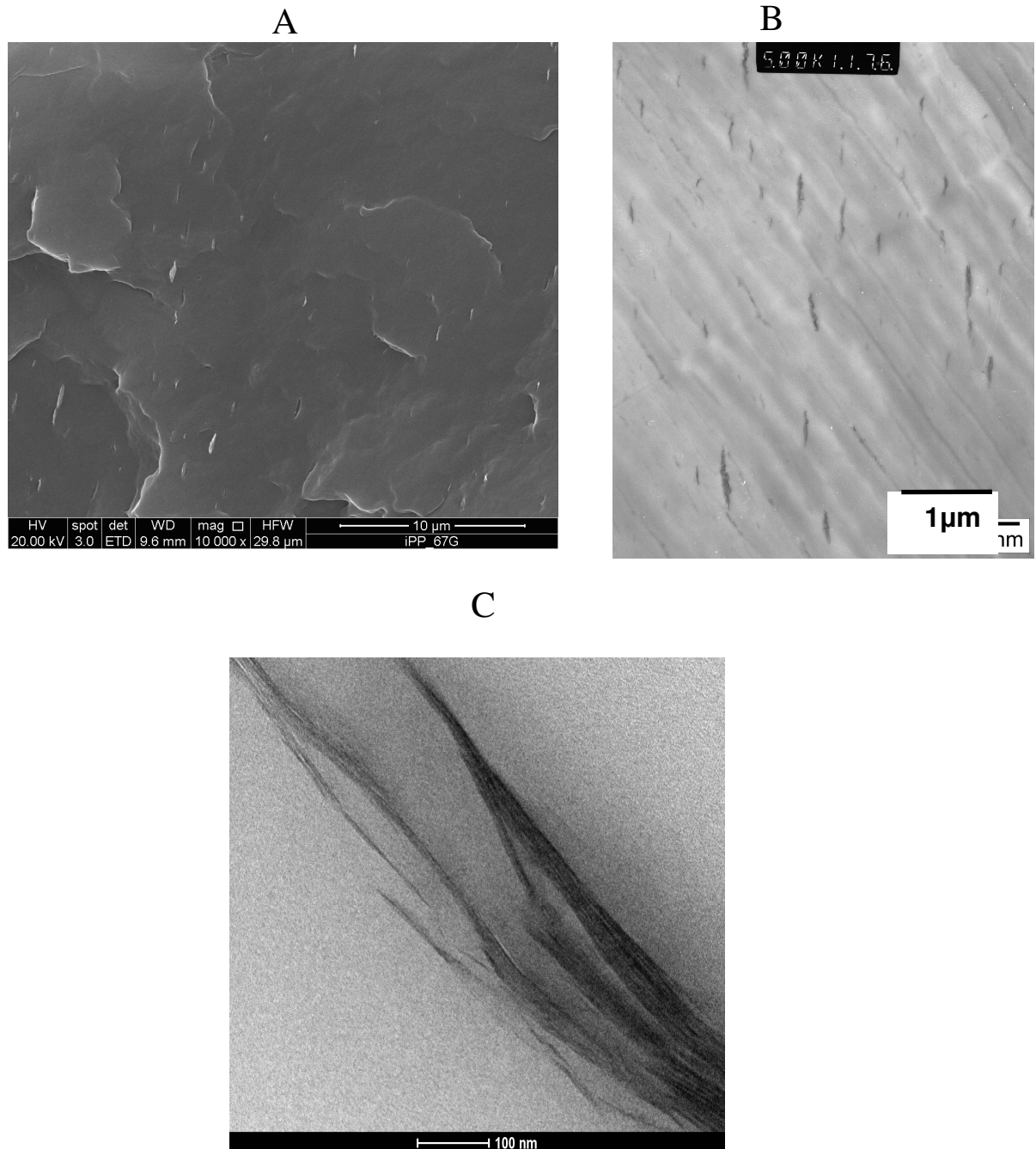
Figure 3: SEM micrograph of iPP/67G at 10000x (A); TEM micrograph of iPP/67G at low magnification (B) and high magnification (C)

For the sample iPP/HPS, the unmodified clay is present in the polymer matrix as big domains as indicated in the figure 4 by the arrow.
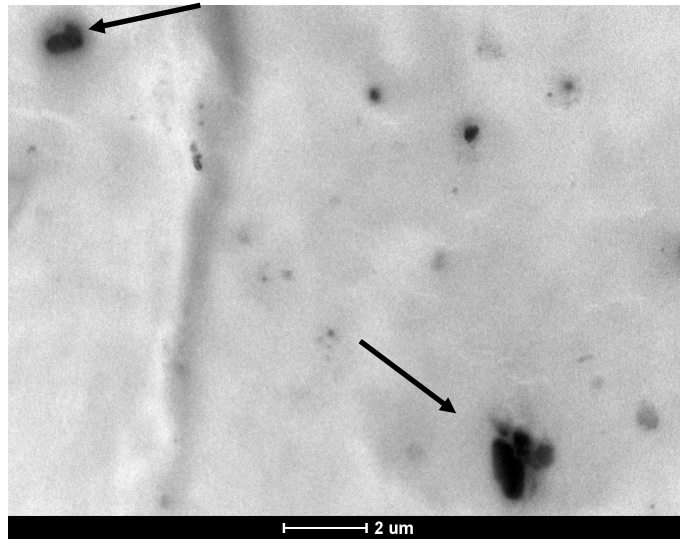
**Figure 4: TEM micrograph iPP/HPS**

Figure 5 shows the micrographs of iPP/ESC5% (A) and iPP/ESC30% (B) at 10000x. For the blends containing 5% of Escorez a homogenous fractured surface is present. That corroborates the hypothesis of compatibility between iPP and Escorez at low content of resin in the blends.

For the system iPP/ESC30% small domains of Escorez are present as indicated in the figure 5 (B) by the arrows.
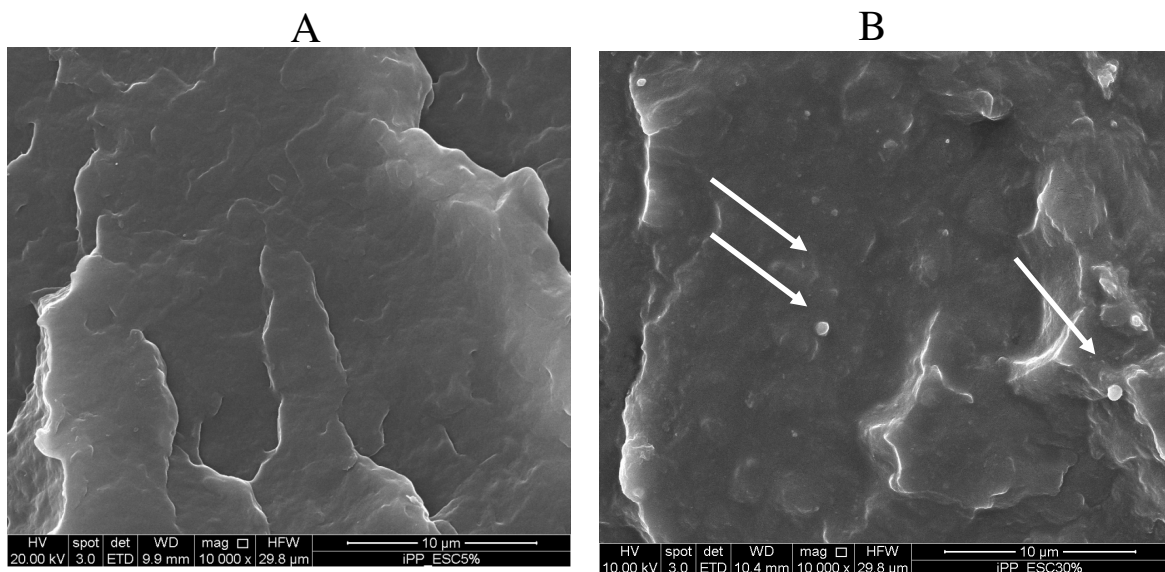
**Figure 5: iPP/ESC5% (A) and iPP/ESC30% (B) at 10000x.**

Figures 6 A, B and C relative to the systems iPP/ESC/Clay, show the same morphology of iPP/67G. In both systems iPP/ESC5%/67G (figure 6 B) and iPP/30%/67G (figure 6 C) small and large tactoids, well distributed, are present (arrows in the figure 6 B and C).
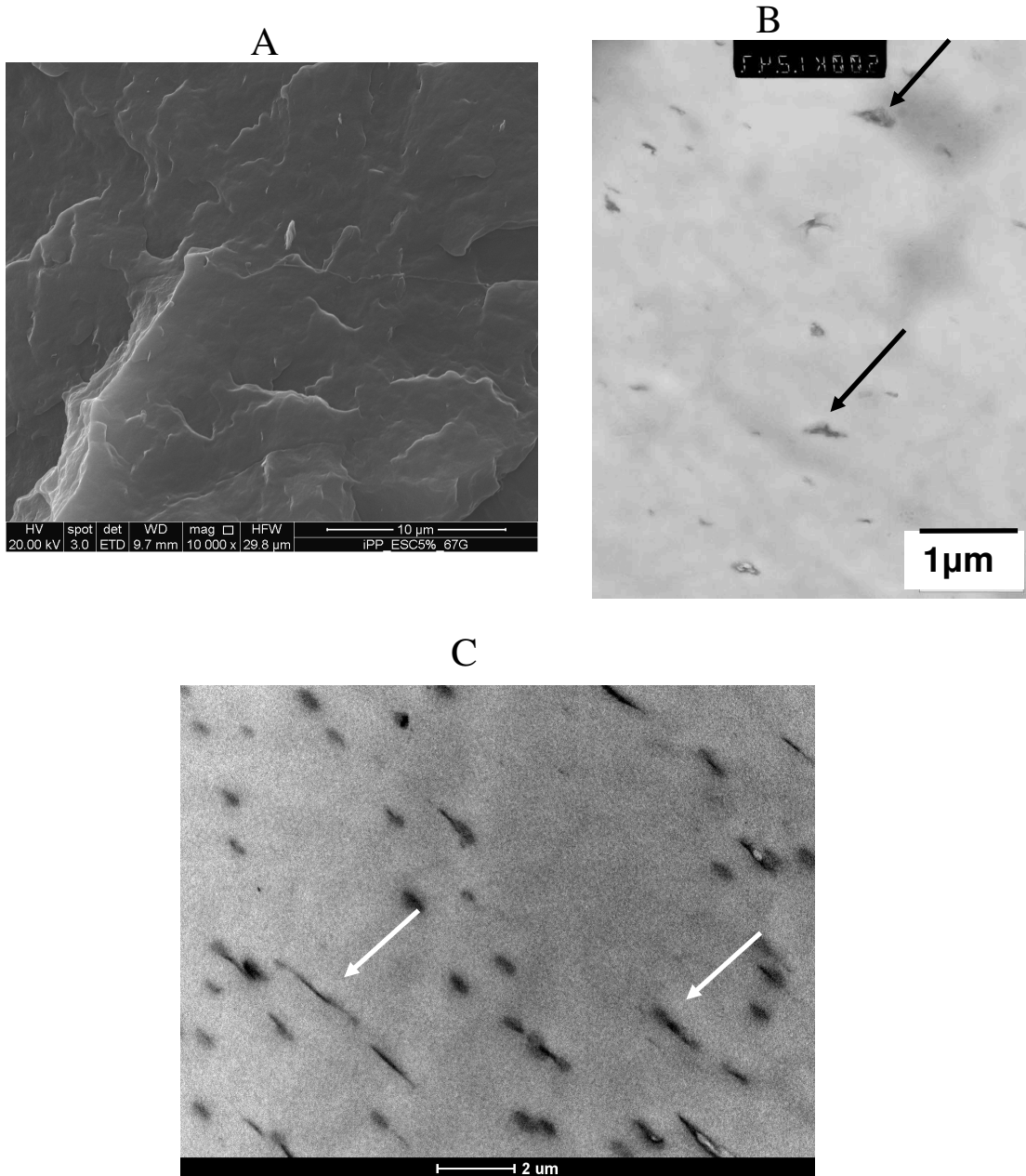
Figure 6: SEM micrograph of iPP/ESC5%/67G at 10000x (A); TEM micrograph of iPP/ESC5%/67G (B) and iPP/ESC30%/67G (C).

The morphology describe up for iPP/ESC blends is also present in iPP/ESC/HPS as shown figure 7 A and B. The presence of Escorez does not modify the distribution of HPS in the

polymer matrix; domains of unmodified clay are still visible in the polymer matrix (arrows in figure 7 C).

A

B

C
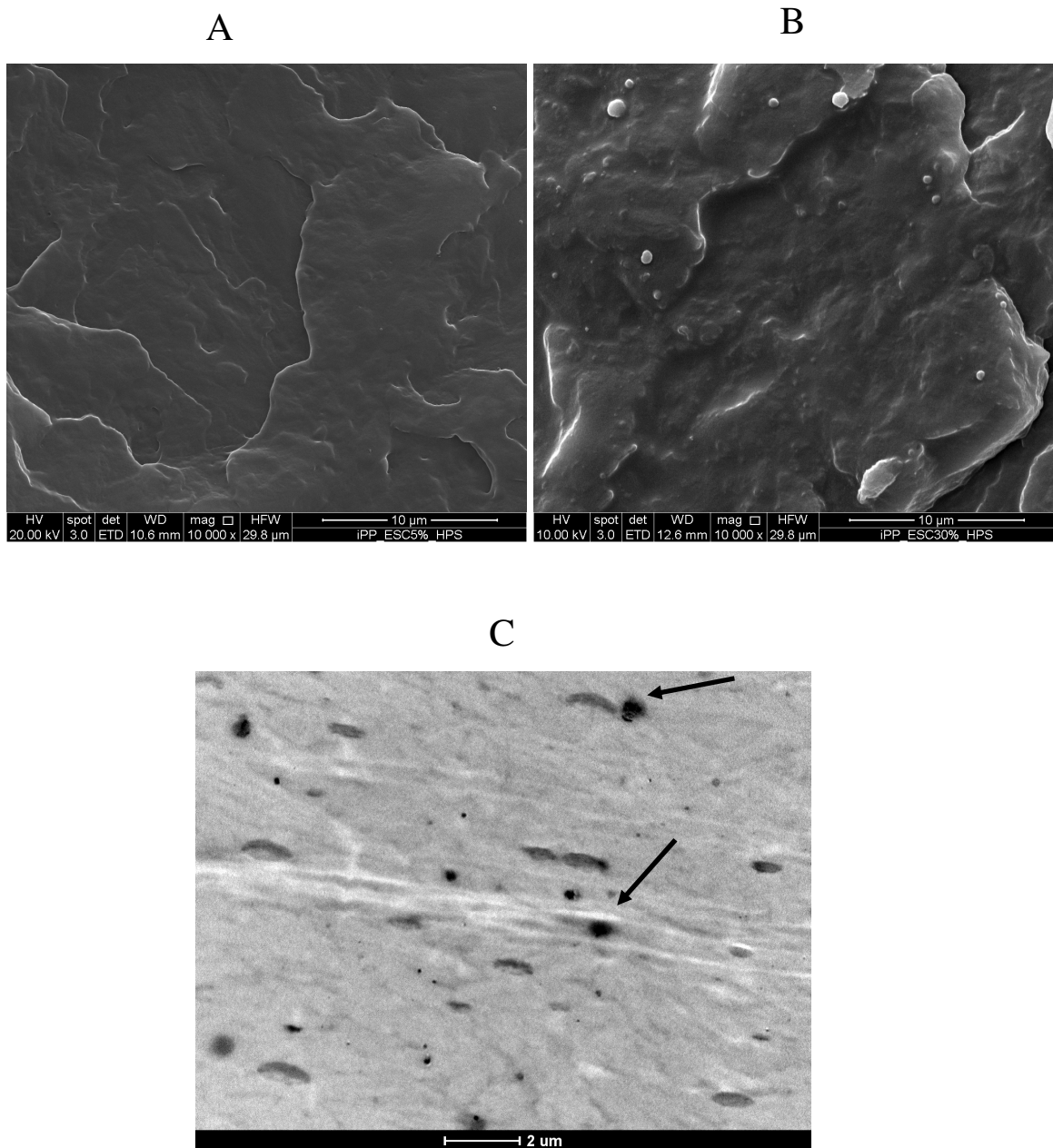
Figure 7: SEM micrographs of iPP/ESC5%HPS (A) and of iPP/ESC30%/HPS (B) at 10000x; TEM micrograph of iPP/ESC30%/HPS (C)

References

(1) Bruckner, S.; Mille, S. V.; Petraccone, V.; Pirozzi, B. *Prog Polym Sci* **1991**, 16, 361.

(2) Silvestre, C.; Cimmino, S.; Di Pace, E. In Handbook of Polyolefins, 2nd ed. ; Vasile, C., Ed.; Marcell Dekker: New York Basel, **2000**; Chapter7.

(3) Cimmino, S.; Silvestre, C.; Duraccio, D.; Pezzuto, M.; *J. Appl.Polym.Sci.,* **2011**, 119, 1135.

(4) Vaia, R. A.; Weathers, M. S.; Bassett, W. A. *Powder Diffraction* **1994**, 9, 44.

Chapter 3

Morphological characterization by SAXS

In this chapter it is reported small angle diffraction patterns of compression molded samples of all systems analyzed in order to study the lamellar morphology of crystalline blends in detail and to extract information on the relative arrangements of the lamellae of the crystalline and amourphous phase.

In figure 1 are reported the desmeared SAXS intensity distribution of as prepared compression molded of iPP, iPP/Clays, iPP/ESC and iPP/ESC/Clay blends.
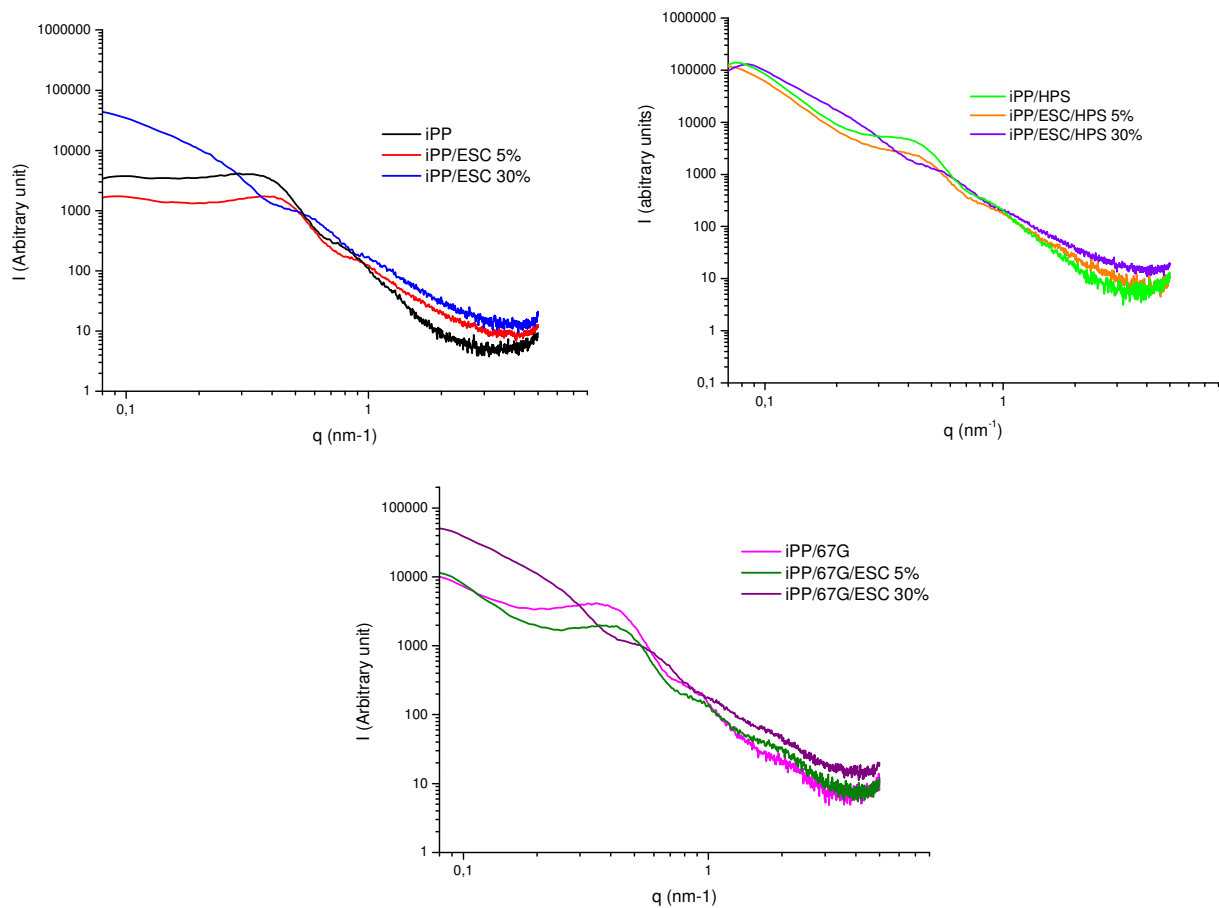
Figura 1: Desmeared SAXS intensity distribution of iPP, iPP/Clays, iPP/ESC and iPP/ESC/Clay blends

In figure 2 the Lorentz-corrected SAXS intensity distribution of pure iPP, iPP/clays, iPP/ESC and iPP/ESC/clay blends are reported. The Lorentz-corrected profiles were calculated by multliplying the SAXS intensity by $q^2/2\pi$. This correction is helpful only for isotropic materials, in our case it indicates that it consists of crystals in which all spatial orientations are present. They show in all cases a correlation peak typical of the lamellar morphology.
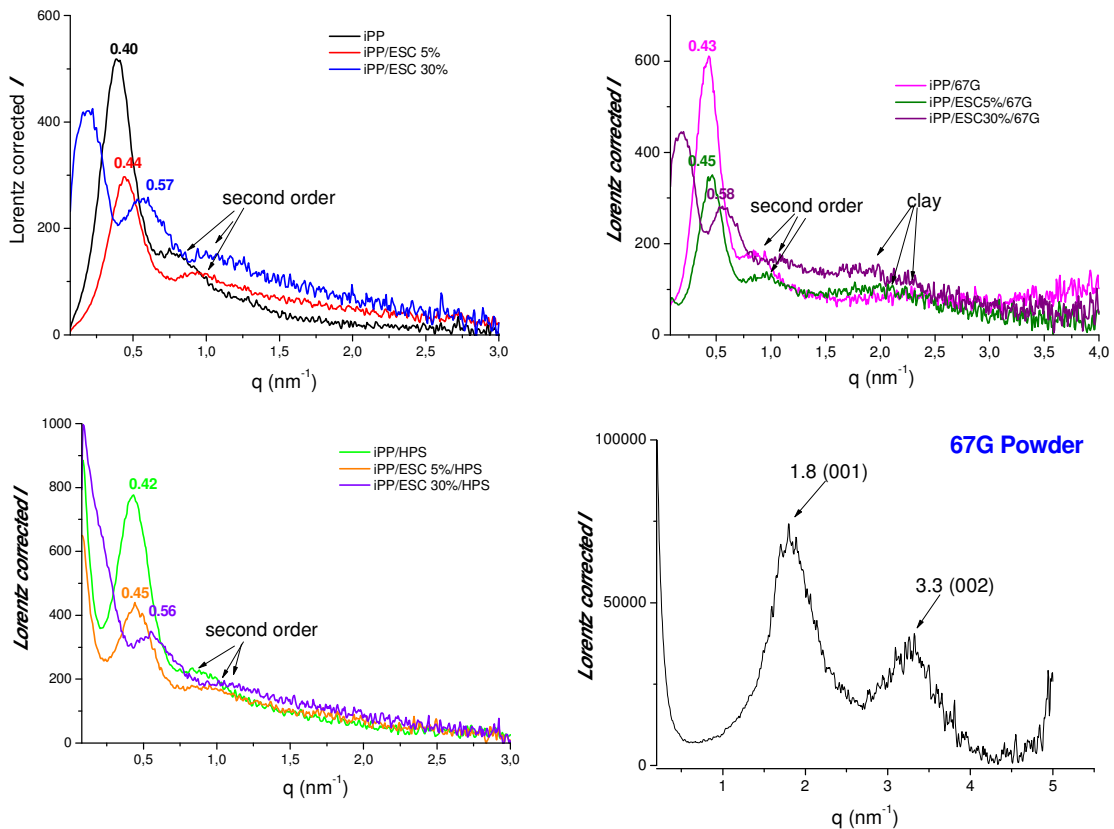
Figura 2: Lorentz corrected SAXS intensity of pure iPP, iPP/clays, iPP/ESC, iPP/ESC/Clay blends and neat 67G powder. The data have been collected at room temperature.

The position of maxima (q^*) of the main SAXS peak of figure 1 are listed in table 1. In particular pure iPP (figure 2) shows a first and second order correlation peak at q= 0.40 and q=0.78 nm^{-1} respectively. For the samples iPP/Clay the first peak is at $q \approx 0.42$ nm^{-1} and the peak corresponding to the second order shifts at $q \approx 0.87$nm^{-1}. Finally the binary and ternary systems containing 5% in weight of Escorez show a first and second order correlation peak at $q \approx 0.45$ and 0.95 nm^{-1} respectively, (figure 2).

Table 1: values of the main peak position (*q**) in the Lorentz corrected SAXS profile of figure 1, Average Long Spacing $\langle L_B \rangle$, Average thickness of crystalline $\langle l_{cB} \rangle$ and amourphous layers $\langle l_{aB} \rangle$ and crystalline degree by WAXD (*x_c*) respect to blend.

Sample	q^* nm^{-1}	$\langle L_B \rangle$ *(nm)*	$\langle l_{cB} \rangle$ *(nm)*	$\langle l_{aB} \rangle$ *(nm)*	x_c(%)(WAXD) blend
iPP	0.40	15.7	10.5	5.2	67
iPP/HPS	0.42	14.9	9.8	5.1	66
iPP/67G	0.43	14.6	9.8	4.8	67
iPP/Esc 5%	0.44	14.3	8.7	5.6	61
iPP/Esc30%	0.58	11.0	5.9	5.1	54
iPP/Esc5%/HPS	0.46	14.0	8.4	5.6	60
iPP/Esc30%/HPS	0.56	11.2	6.0	5.2	54
iPP/Esc5%/67G	0.46	14.0	8.5	5.5	61
iPP/Esc30%/67G	0.58	10.8	5.9	4.9	55

The SAXS profile (figure 2) of blends containing 30% of Escorez shows two peaks at $q \approx$ 0.19 and 0.56 nm^{-1}, *Silvestre at al.* found that two kinds of crystallite formed by lamellae of iPP and amorphous material rich in iPP and Escorez respectively, are present;[1] for these blends no definite second order correlation peak is present but only a broad halo centered at $q \approx 1$ nm^{-1}.

In all the blends containing 67G a broading peak centered at $q \approx 1.9$ nm^{-1} is present. The (001) plane peaks of 67G in the same position of the SAXS profile of pure powder 67G indicates that the iPP does not intercalate into 67G layers.

From the peak position q^*, the average value of the long period $\langle L_B \rangle$ can be obtained $\approx 2\pi/q^*$, where subscript B indicates that it has applied the Bragg law for the evaluation of this parameters.

For all the samples the $\langle L_B \rangle$ value decreases with improving the content of Escorez in the blends.

The values of $\langle L_B \rangle$, in turn , can be used for an evaluation of the average thickness of crystalline and amorphous layers, $\langle l_{cB} \rangle$ and $\langle l_{aB} \rangle$ respectively given by $\langle l_{cB} \rangle \approx \langle L_B \rangle * x_c$ *(WAXD)* and $\langle l_{aB} \rangle \approx \langle L_B \rangle - \langle l_{cB} \rangle$. The value of $\langle L_B \rangle, \langle l_{cB} \rangle$ and $\langle l_{aB} \rangle$ are reported in table 1.

The $\langle l_{cB} \rangle$ value decreases with Escorez content. It is possible that the presence of Escorez disturbs the iPP crystallization process. In particular, the Escorez causes a reduction of the spherulite growth rate as it acts as diluent for the iPP, inducing an increase of the energies related to the formation of a nucleus of critical size and to motion of macromolecules in the growing crystals, in agreement with the crystallization theory of polymer blends[1].

The average thickness of amorphous phase $\langle l_{aB} \rangle$ of iPP (5.2 nm^{-1}) is not perturbated by the presence of HPS. Whereas in the presence of 67G, the iPP $\langle l_{aB} \rangle$ decreases from 5.2 to 4.8 nm^{-1}. The average thickness of amorphous phase in between the crystalline lamellae $\langle l_{aB} \rangle$ of the blends containing 5% of Escorez (5.6 nm^{-1}) increases respect to the neat iPP $\langle l_{aB} \rangle$ value (5.2 nm^{-1}).

For the samples iPP/ESC30% and iPP/ESC30%/HPS the $\langle l_{aB} \rangle$ value is 5.2 nm^{-1} as $\langle l_{aB} \rangle$ value of pure iPP. That could be explained because in this case the calculation have been performed by using the only value of the peak formed by lamellae of iPP and amorphous material rich in iPP.

Under the classical assumption that stacks of lamellae may be approximated by a monodimensional array of alternating crystalline and amourphous layers of finite thickness and lateral dimension much higher than the thickness of the two layers arranged parallel each other, it is possible to apply the autocorrelaction function of electron density fluctuations normalized by the scattering invariant [2] (equation 1)

$$p(r) = \frac{1}{Q} \int_0^\infty \left(I(q) - I_{back} \right) q^2 \cos(qr) dq \quad \text{(Eq.1)}$$

where r is the direction along which the electron density is measured. The numerator is Fourier transformation of SAXS intensity on all the volume busy by the sample and the denominator is the scattering invariant Q calculated as

$$Q = \int_0^\infty \left(I(q) - I_{back} \right) q^2 dq \quad \text{(Eq 2)}$$

In the assumption that SAXS intensity probes heterogeneities arising from a simple two phase structure at nanometer length scale, the SAXS desmeared data, after subtraction of the residual background intensity (approximated as a costant I_b) has been extrapolated to high q values with the aid of the Porod law [3], in the hypothesis of no diffuse boundary between crystalline and amorphous layers, i.e. by fitting the experimental data in the high q region with the equation:

$$\lim_{q \to \infty} I(q) - I_{back} = K_p q^{-4} \quad \text{(Eq 3)}$$

Where K_p is a quantity proportional to the Porod constant P through a factor K due the fact that our intensity is in relative units.

For the extrapolation to q=0 of SAXS desmeared data we have used the Debye-Bueche equation[4]:

$$I(q) - I_{back} = \frac{B}{\left(1 + C^2 q^2\right)^2} \quad \text{(Eq.4)}$$

where B and C are interpolation parameters.

The correlation function has been used in order to obtain the average value of long spacing (L), of lamellar thickness (l_c), of thickness of amorphous layers (l_a) and of linear crystallinity grade SAXS (X_c(SAXS)= (l_c /L)*100) for all the samples analysed.

In figure 3 the correlation function (*p(r)* vs *r*) of as prepared compression molded samples of pure iPP, iPP/Clay, iPP/ESC and iPP/ESC/Clay blends are reported.

Determinations of l_c, l_a , and L may be realized by locating the first minimum and maximum in the one-dimensional correlation function[2]

L is related to the abscissa of the maximum of *p(r)*. In the initial slope region, called the "self-correlation region", the curve shape accounts for the dimensions of the lamellae and the interface. The thickness of one phase can obtained from intercept values between the tangent to at low *r* and the tangent to the minimum of the correlation function *p(r)*. When the *x*c by WAXD is smaller than 50 %, the value of intercept corresponds to l_a and then the lamellar spacing l_c= L- l_a.

In table 2 are reported the comparison of morphological parameters obtained by applying correlation function and Lorentz corrected SAXS profile.

Long spacing value (*L*) calculated by correlation function is in a good agreement with the long period $\langle L_B \rangle$ calculated by Lorentz corrected SAXS profile.

l_c value for iPP/Clays and the binary and ternary systems containing 5% of Escorez is similar to that one of pure iPP. For the blends containing the 30% of Escorez l_c value is $\approx$ 7.3 nm respect to 11,6 nm of neat iPP.

The presence of 67G and HPS does not modify the thickness of amorphous layers l_a of iPP; otherwise the presence of Escorez in the all blends reduces the l_a value.

Linear degree of crystallinity calculated x_c by SAXS analysis is greater to linear degree of crystallinity calculated by WAXS analysis. That is in agreement with that SAXS estimates

local crystallinity from the lamellar stacks and take in account only intra–lamella amorphous, while WAXS data provide bulk crystallinity and the global amorphous in the samples. For all the samples the x_c (SAXS) is similar to pure iPP with exception of blends containing 5% of Escorez where the x_c (SAXS) increases respect to pure iPP.
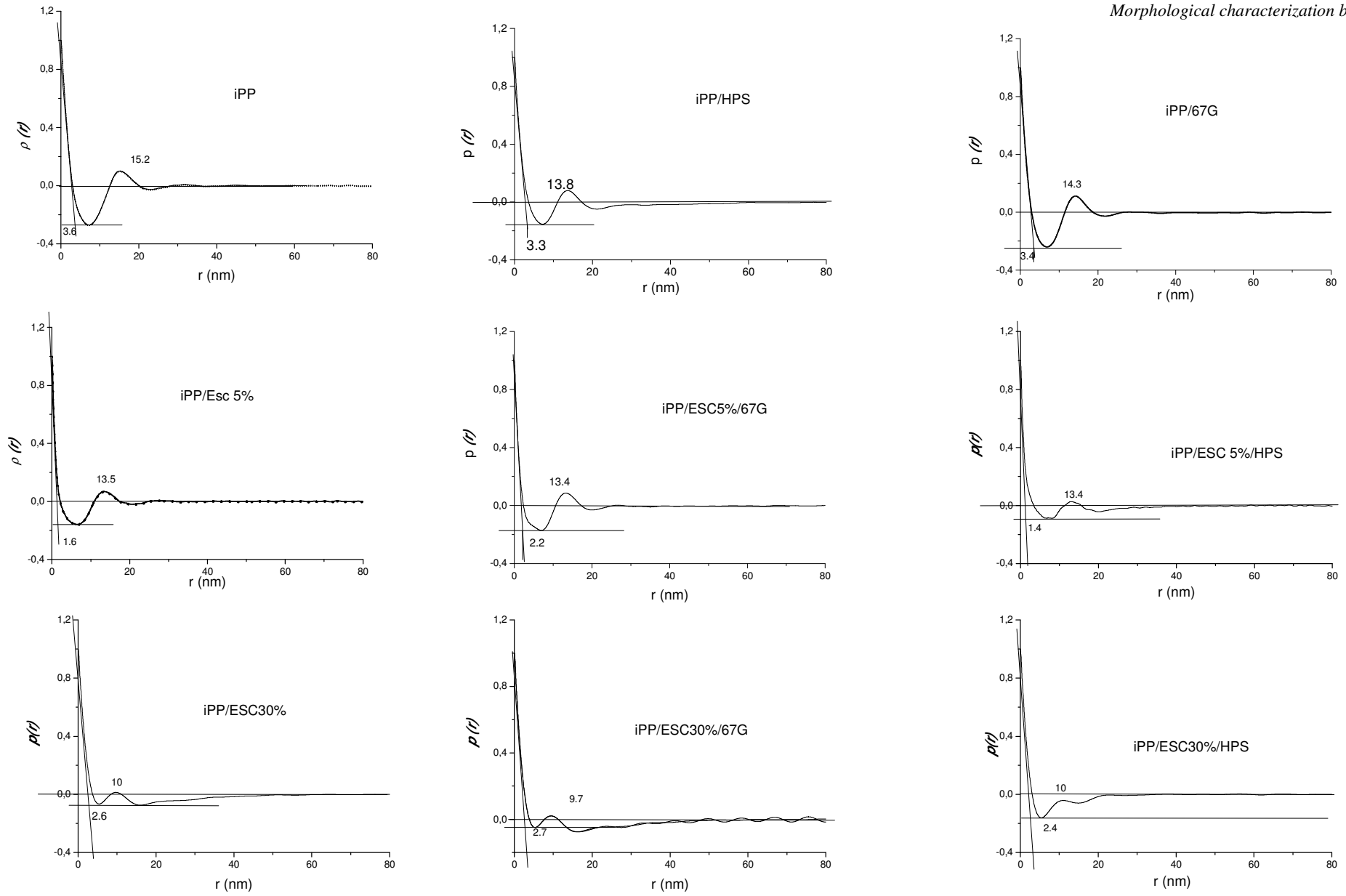
Figure 3: The correlaction function (*p(r)* vs *r*) of as prepared compression molded samples of pure iPP, iPP/Clay, iPP/ESC and iPP/ESC/Clay blends

Table 2: Comparison of morphological parameters obtained by applying correlation function and Lorentz corrected SAXS profile of as prepared compression moulded samples

Sample	$\langle L_B \rangle$ (nm)	$\langle l_{cB} \rangle$ (nm)	$\langle l_{aB} \rangle$ (nm)	L (nm)	l_c (nm)	l_a (nm)	x_c (%) (WAXD)	x_c (%) (SAXS)
iPP	15.7	10.5	5.2	15.2	11.6	3.6	67	76
iPP/HPS	14.9	9.8	5.1	13.9	10.6	3.3	66	76
iPP/67G	14.6	9.8	4.8	14.3	10.9	3.4	67	76
iPP/Esc 5%	14.3	8.7	5.6	13.5	12.1	1.4	61	89
iPP/Esc30%	11.0	5.9	5.1	10	7.3	2.7	54	73
iPP/Esc5%/HPS	14.0	8.4	5.6	13.4	12	1.4	60	88
iPP/Esc30%/HPS	11.2	4.4	6.8	10	7.6	2.4	54	76
iPP/Esc5%/67G	14.0	8.5	5.5	13.4	11.2	2.2	61	84
iPP/Esc30%/67G	10.8	5.9	4.9	9.7	7.1	2.6	55	73

References

(1) Triolo, A.; Silvestre, C. Cimmino, S.; Martuscelli,E.; Caponetti,E. and Triolo,R. *Polymer*, **1998**, 39, 1697.

 (2) Strobl, G. R.; Schneider, M. *J. Polym. Sci.: Polym. Phys. Ed*. **1980**, 18, 1343

(3) Roe, R.J. *Methods of X-ray and neutron Scattering in Polymer Science*; Oxford University Press: New York, 2000; Koberstein, J. T.; Morra, B.; Stein, R.S. *J.Appl. Crystallogr*. **1980**,13,34.

(4) Debye, D.; Beuche, A.M. *J. App. Phys.* **1949**, 20, 518.

<div align="center">

Chapter 4

Calorimetric analysis

</div>

4.1 Melting behaviour

Differential scanning calorimetry (DSC) has been widely applied in investigations of numerous phenomena occurring during thermal treatment of organoclays and polymer-clay nanocomposites, involving melting, crystallization, and glass transition.

Thermo-analytical curves of compression-molded iPP, iPP/ESC and nanocomposites are reported in Figure 1. About 10 mg of the sample was heated from -80 °C to 200 °C at a rate of 10 °C/min, after cooling at 20 °C/min, the sample was heated again from -80 °C to 200°C (reported run) at a rate of 10 °C/min. The thermograms of 2nd run are not reported in figure 1: they show the same qualitative behaviour of the 1st run.

The thermograms present only one endothermic transition due to the melting of monoclinic crystals of iPP. The melting temperature values of the first $(T_m$ (1st Run)) and second run $(T_m$ (2nd Run)) are reported in Table 1. A slight decrease in the T_m maximum peak of iPP is noticed when the Escorez content is 30% in blends. The decrease of T_m can be due to two factors: (i) kinetic effect; (ii) thermodynamic effect [1,2]. Considering that for these compositions it is found a T_g increase (see Table 1), due to the partial compatibility[3] between iPP and Escorez, it can be concluded that both the factors contribute to decrease of the T_m.
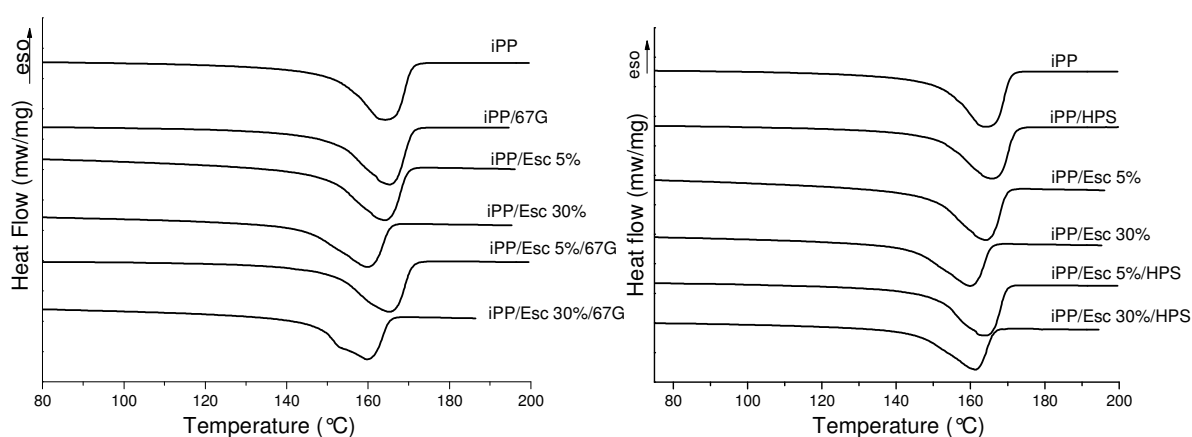
Figura 1 : Thermo-analytical curves of 1st run

The glass transition temperature of the first run $(T_g$(1st Run)) for iPP, iPP/Clay, iPP/ESC and iPP/ESC/Clay blends pointed out by the first derivative curves, is shown in figure 2.
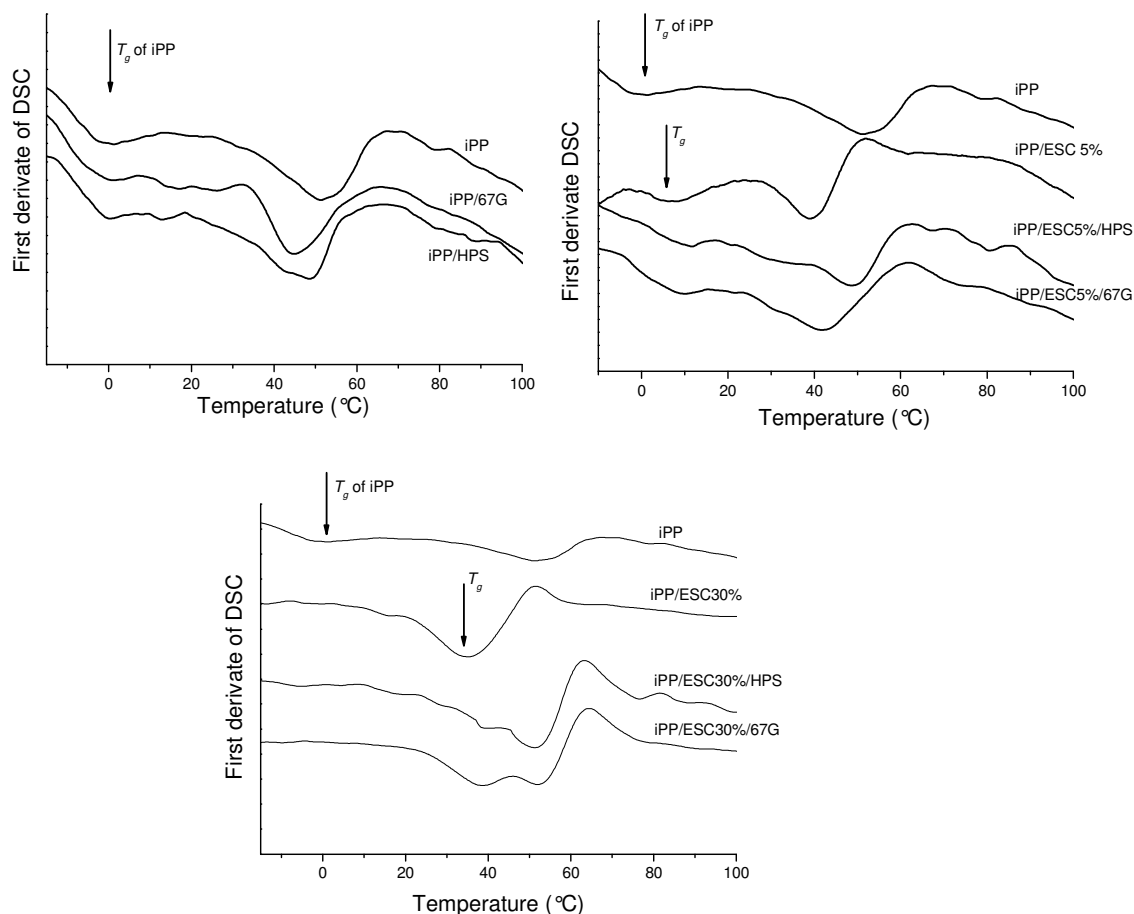
Figure 2: Glass transition temperature (T_g (1st Run) for iPP, iPP/Clay, iPP/ESC and iPP/ESC/Clay blends.
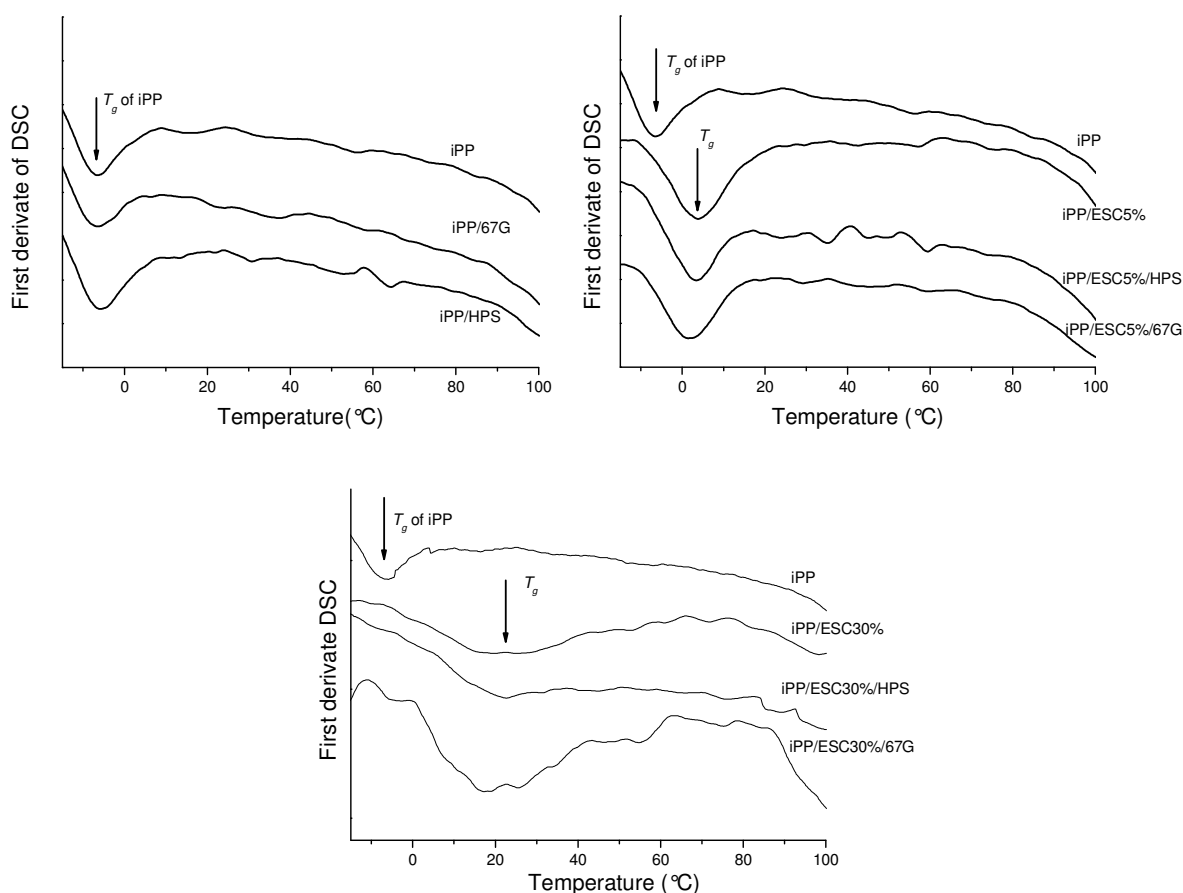
The T_g(1st Run) value of iPP/HPS and iPP/67G composite are similar to that of plain iPP. For the blends containing 5% of Escorez the T_g (1st Run) increase of 8-11° (see table 1) due the compatibility between iPP and Escorez in amorphous phase, according to the phase diagram. [4]

The blends with Escorez content less than about 20% (w/w) should always form a homogenous melt. Even at room temperature, these blends are characterized by crystalline in miscible amourphous phase formed by non-crystalline iPP and Escorez. [4]

For blends containing the 30% of Escorez, phase separated melt can be obtained depending on temperature. [4] For this composition glass transition temperature shifts to higher value respect that of iPP. No other transition to attribute the rich Escorez amourphous phase at higher value of temperature are detectable on first derivate of thermograms (Figure 2 B-C). For these reasons, from DSC it is possible to deduce that iPP and Escorez are compatible in the amorphous phase. However by SEM analysis the presence of small domains attributed of Escorez are found. As on the DSC thermogram of iPP/ESC30% only one T_g is present, it can

be concluded that the transition of ESC domains visible by SEM (expected to be in the range 80-90 °C) is not detectable because this phase amount is too small and behind the DSC sensibility.

The glass transition temperature of the second run (T_g(2nd Run)), for iPP, iPP/Clay, iPP/ESC and iPP/ESC/Clay blends that pointed out by the first derivative curves, is shown in figure 3 and reported in table 1.

Figure 3: Glass transition temperature of the second run T_g (2nd Run) for iPP, iPP/Clay, iPP/ESC and iPP/ESC/Clay

Analogue to the first run the T_g(2nd Run) value of iPP/HPS and iPP/67G composite are similar to that plain iPP. For the blends containing 5% a single value of glass transition temperature confirms a compatibility between amorphous phase of iPP and Escorez and for the blends containing 30% of Escorez a clear peak at 20°C is detectable.

The value of heat of fusion, measured by DSC method and reported in table 1, is commonly used to calculate the degree of crystallinity. A decrease of degree of crystallinity calculated respect to the blend iPP/ESC occurred proportionality to the amount of content of Escorez in all blends (shown in table 1). The addition of clays does not modify the value of degree of crystallinty compared with the neat iPP in the binary systems and also in the ternary systems

compared to that of iPP/ESC blends. The value of X_c respect to iPP phase is almost the same in all samples.

| Table 1: values of melting temperature T_m (1st Run) and T_m (2nd Run) of first and second run respectively; value of glass transition (T_g(1st Run)) and T_g(2nd Run) of first and second run respectively; heat of fusion ΔH (J/g); degree of crystallinity for all samples X_c respect to the blends and to iPP phase.						
Sample	T_m (1st Run) (°C)	T_g(1stRun) (°C)	T_m (2ndRun) (°C)	T_g(2nd Run) (°C)	ΔH (J/g)	X_c (DSC) ±2 blends	X_c (DSC) ±2 iPP Phase
iPP	165	0	165	-6	93	44	44
iPP/HPS	166	0	166	-5	93	45	45
iPP/67G	164	1	164	-6	93	45	45
iPP/ESC5%	164	8	164	4	81	39	41
iPP/ESC30%	160	35	160	22	61	30	43
iPP/ESC5%/HPS	164	11	164	3	82	40	42
iPP/ESC5%/67G	165	10	165	3	86	41	43
iPP/ESC30%/HPS	161	39	161	22	64	31	44
iPP/ESC30%/67G	160	39	160	22	67	32	46

4.2 Non-isothermal crystallization

The DSC scans recorded during non-isothermal crystallization of investigated samples at cooling rate from 5 to 20°C/min are given in figure 2, 3 and 4. Table 2 reports the crystallization temperature (T_c) at different cooling rate measured at the maximum of the esothermic peaks.
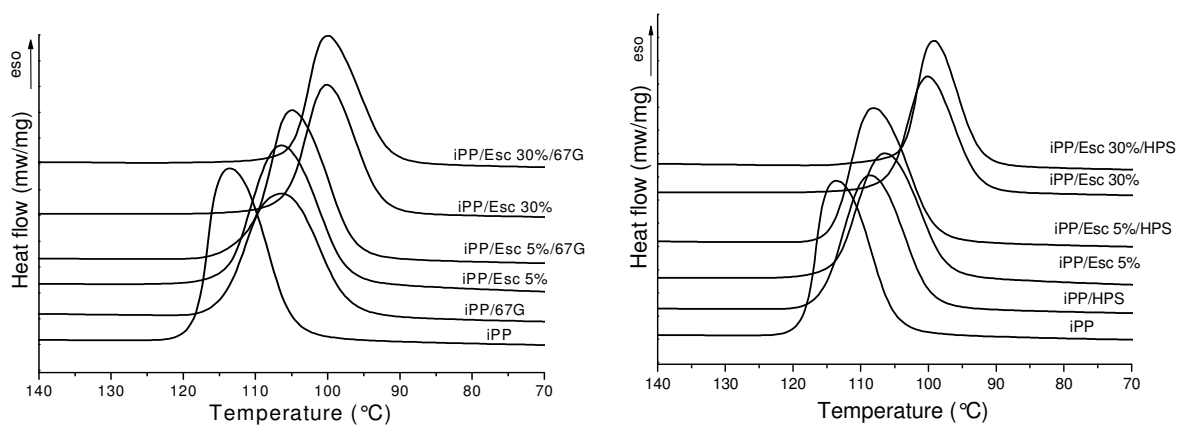
Figure 2 : Non-isothermal crystallization of investigated samples at cooling rate of 20°C/min
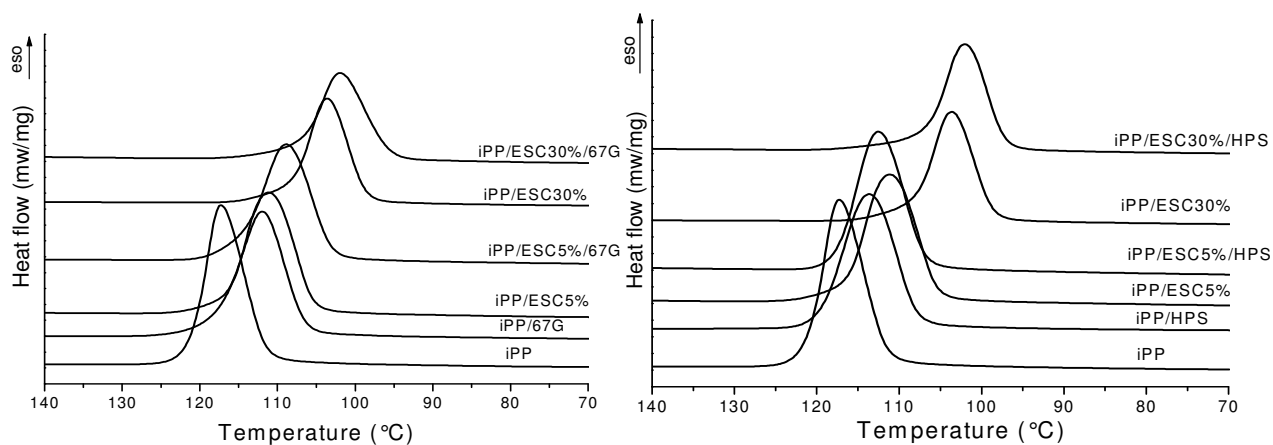
Figure 3: Non-isothermal crystallization of investigated samples at cooling rate of 10°C/min
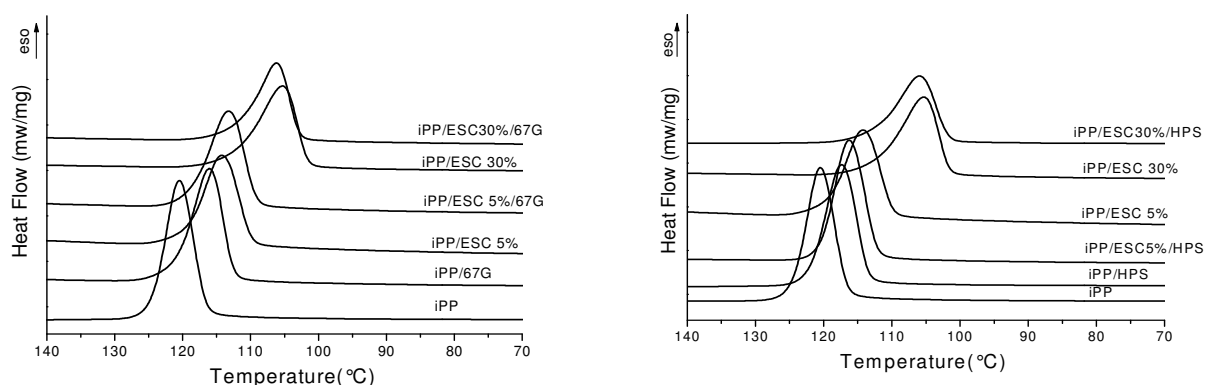
Figure 4 : Non-isothermal crystallization of investigated samples at cooling rate of 5°C/min

The non crystallization behaviour in quiescent conditions depends on composition and cooling rate: at a given cooling rate for all the samples the crystallization process shifts to lower temperatures with respect to plain iPP. For a given sample increasing the cooling rate the crystallization process starts at lower temperatures. Both the increase of cooling rate and the addition of clay and/or ESC shifts the crystallization onset to lower values indicating that the nucleation process occurs at lower temperature. In the case of blends containing ESC the influence is depending on composition. These results can be attributed to the diluent effect of ESC (for the binary and ternary blends containing ESC) and to the presence of clay particles that effect the transport of macromolecules chains toward the growing nuclei.

Table 2: crystallization temperature (T_c °C) at different cooling rate

| Sample	T_c (20°C/min)	T_c (10°C/min)	T_c (5°C/min)
iPP	114	117	120
iPP/HPS	108	113	117
iPP/67G	106	112	116
iPP/Esc 5%	106	111	114
iPP/Esc 30%	100	103	105
iPP/Esc5%/HPS	108	113	116
iPP/Esc 5%/67G	105	109	113
iPP/Esc30%/HPS	99	102	105
iPP/Esc30%/67G	100	102	106

References

(1) Nishi, T.;. Wang, T.T. *Macromolecules* **1975**, 8, 909.

(2) Silvestre, C.; Cimmino, S.; Di Pace, E. 'Morphology of Polyolephins' in Handbook of Polyolephins, 2nd Edition, revised and expanded, Ed. C. Vasile, Marcel Dekker, NY, USA, **2000**, Chapter 7, pp. 175.

(3) Maiti, P.; Nam, P.H.; Okamoto, M.; Kotala, T.; Hasegawa, N.; Usuki, A. *Polym. Eng. Sci*. **2002**, 42, 1864.

(4) Cimmino, S.; Di Pace, E.; Karasz, F. E.; Martuscelli, E. and Silvestre C. *Polymer*, **1993**, 34, 972.

Chapter 5

Termogravimetric analysis

The effect of the Escorez and clay presence on the thermal stability of the composites was studied by means of thermogravimetry experiments carried out in both inert and oxidative conditions. The temperature corresponding to initial 10% of weight loss (T_{10}), the temperature of maximum rate of weight loss (T_{mr}), obtained by TGA (figure 1, 3) and DTG (figure 2,4) experimental curves, are given in table 1.
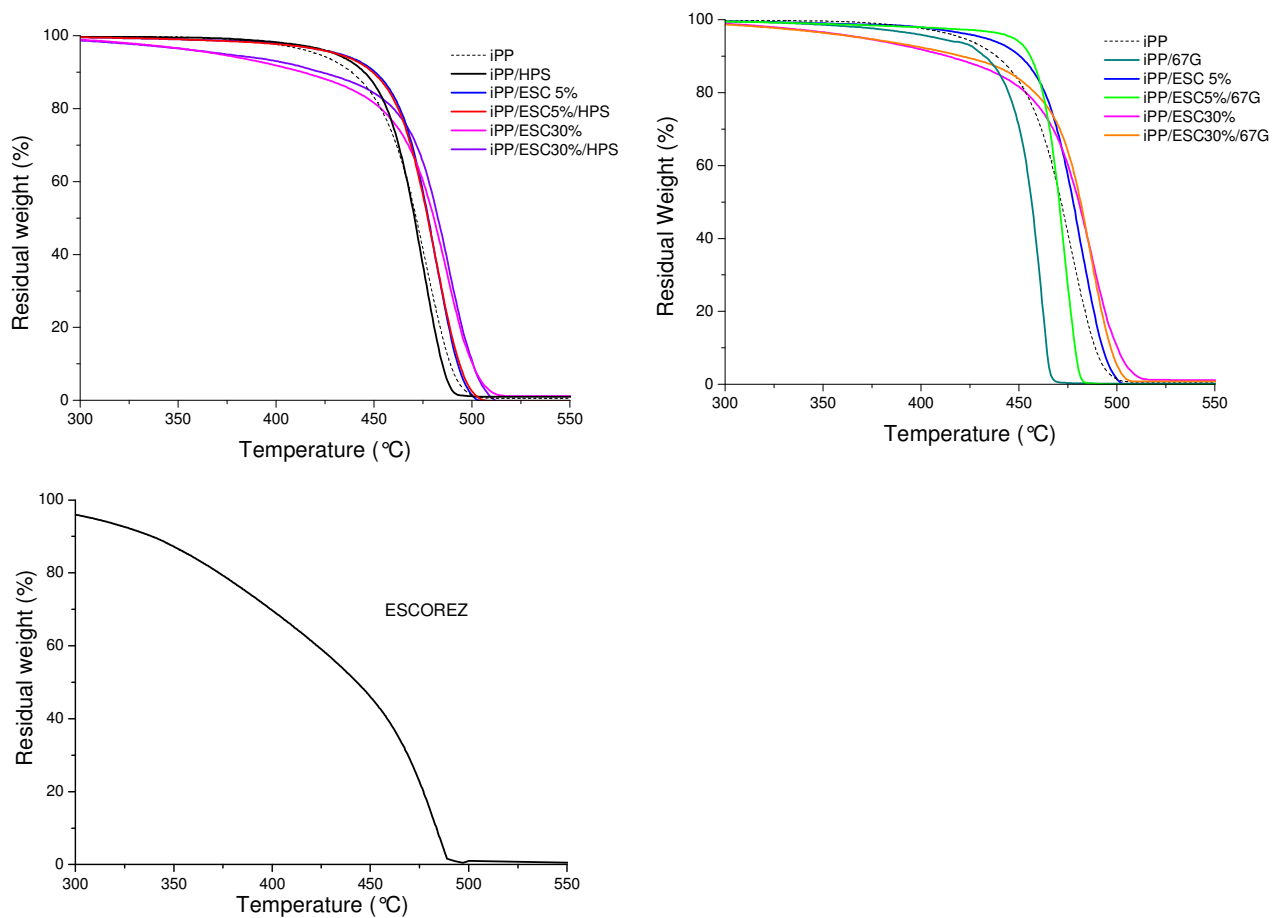

Figure 1: TGA curves under nitrogen (heating rate of 20°C/min) of compression molded samples and neat Escorez

During the thermal degradation in inert atmosphere all the samples show a single step of degradation (figure 1 and 2). For all the samples containing 30%, with and without clay, it is observed that the initial weight loss begins at lower temperatures than that for pure iPP.
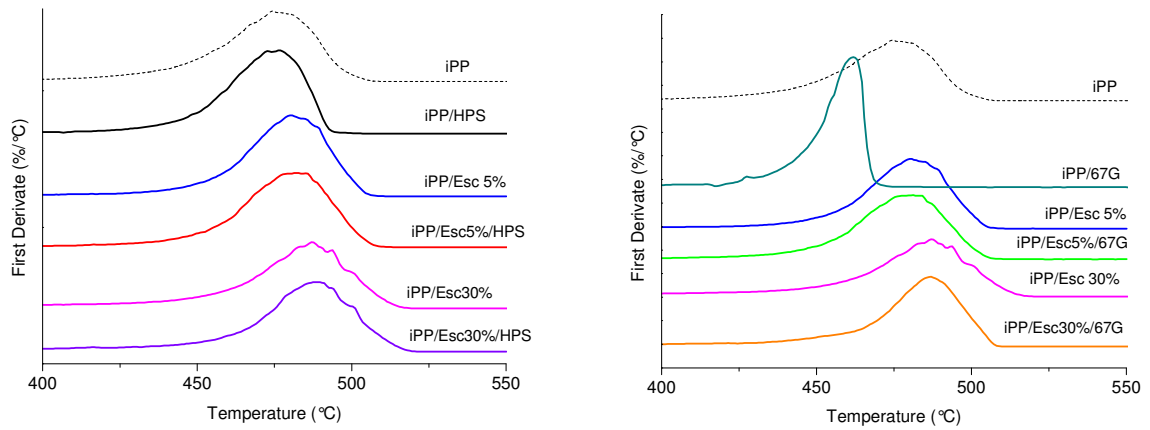
Figure 2: DTG curves under nitrogen of compression molded samples

This behaviour is probably due to the big amount of ESC that presents a broad degradation region starting from about 300°C (figure1) associated with the evolution of organic products. However the T_{mr} for these compositions are higher than that of iPP. The presence of the HPS does not affect the thermal stability of iPP, whereas a small decrease of T_{10} and T_{mr} is observed for 67G. Moreover for iPP/67G the overall degradation process is faster than that of the other systems (figure 2 right side). This behaviour could be ascribed to the presence of acidic sites on modified layer silicates, formed after the Hoffmann degradation, which catalyse the polymer degradation. [1]
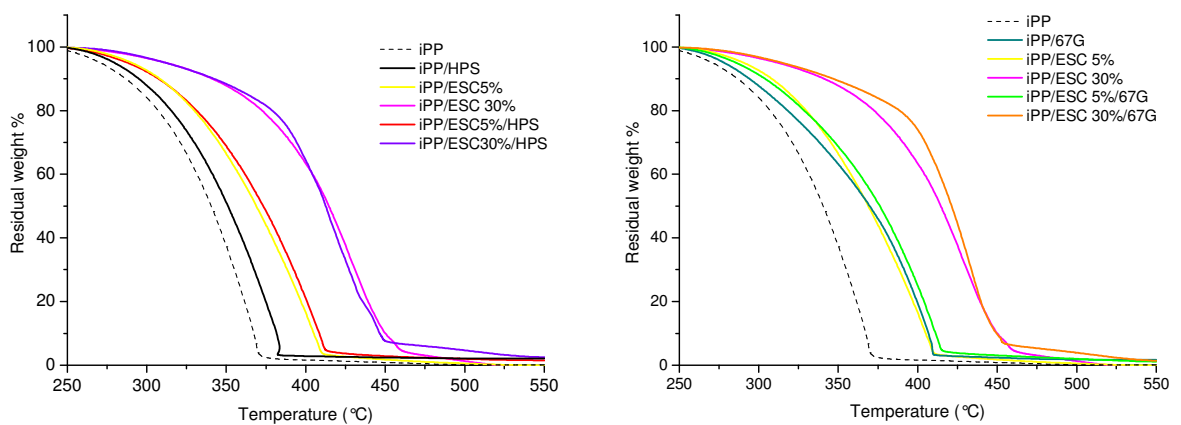
Figure 3: TGA curves in air at heating rate of 20°C/min
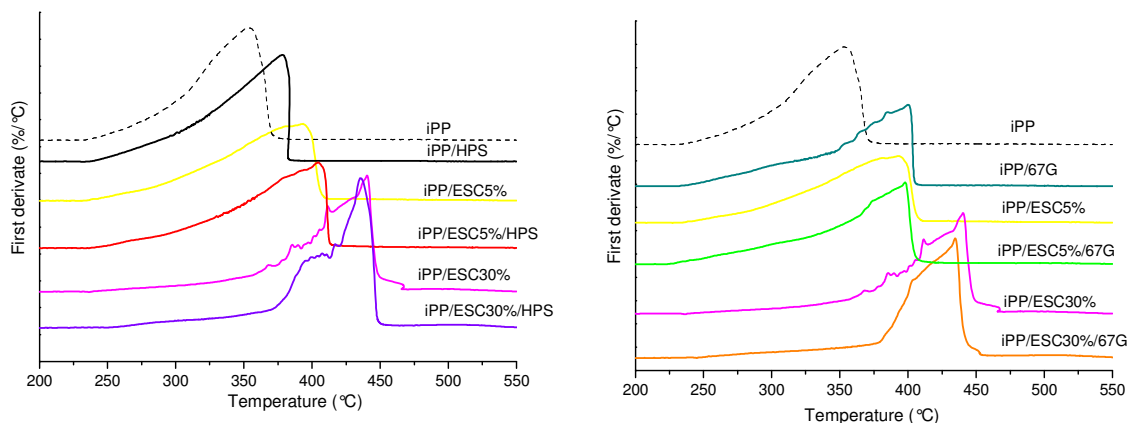
Figure 4: DTG curves in air at heating rate of 20°C/min

Anyway in literature there have been reported opposite behaviours in terms of reduction, [2,3] or improvement, [1,4,5] of the thermal stability in inert atmosphere of iPP nanocomposites. Finally, no significant differences are detectable for the other compositions respect to neat iPP in inert conditions.

Figures 3 and 4 report the TGA and DTG curves, obtained under air atmosphere, of iPP composites. The thermo-oxidative degradation of pure iPP takes place in one stage from 235 to 380°C. It is known that iPP degrades to volatiles products above 250°C trough a radical chain process propaged by carbon centred radicals originated by carbon-carbon scission. [6] For all the other composites a more complex process takes place.

The addition of clay (both HPS and 67G) slightly increases the thermal stability of iPP. The effect is a little more evident for 67G (figure 4). In particular for iPP/HPS and iPP/67G the T_{10} is 295 and 293°C respectively compared to 286°C recorded for pure iPP and T_{mr} is 377 and 400°C respect to 351°C for iPP. This small increase in thermal stability is probably due to a physical barrier effect of the silicate layers. The barrier effects concerns the diffusion of the volatile thermal oxidation products to the gas phase and, at the same time, of the oxygen from the gas phase to the polymer matrix. The samples containing ESC (5 and 30%) show a significant increase of thermal stability in air , in terms of T_{10} and T_{mr} temperatures compared to the pure iPP. The increase is proportionally to the amount of Escorez. It is possible that Escorez acts as a stabilizer for iPP in the blend by retarding the autocatalytic propagation of carbon radicals. The addition of clay to iPP/ESC blends does not affect significantly more the thermal stability of these blends.

Table1: Temperature of residual weight at 10% *(T$_{10}$)*; Temperature at which the maximum weight loss rate is reached *(T$_{mr}$)*

|	Nitrogen		Air	
Sample	T_{10} (°C)	T_{mr} (°C)	T_{10} (°C)	T_{mr} (°C)
iPP	438	477	286	351
iPP/HPS	444	475	295	377
iPP/67G	423	461	294	400
iPP/Esc5%	450	481	308	388
iPP/Esc30%	413	488	341	440
iPP/Esc5%/HPS	449	482	306	403
iPP/Esc5%/67G	456	480	303	397
iPP/Esc30%/HPS	423	486	341	436
iPP/Esc30/67G	421	486	347	434

References

(1) Zanetti, M.; Camino, G.; Reichert, P.; Mülhaupt. *Macromol. Rapid Commun*. **2001**, 22,176.

(2) Tidjani, A.; Wald, O.; Pohl, M.M.; Hentschel, M.P.; Schartel, B. *Polym Degrad Stab.* **2003**, 82, 133.

(3) Wang, D.; Wilkie, C. *Polym Degrad Stab* **2003**, 80, 171.

(4) Tang, Y.; Hu, Y.; Song, L.; Zong, R.; Gui, Z.; Chen, Z. *Polym Degrad Stab* **2003**, 82, 127.

(5) Qin, H.; Zhang, S.; Zhao, C.; Feng, M.; Yang, M.; Shu, Z. *Polym Degrad Stab* **2004**, 85, 807.

(6) Grassie, N.; Scott, G. *Polymer degradation and stabilization,* Cambridge University press, Cambridge **1985.**

Chapter 6

Mechanical and Barrier Properties to oxygen

6.1 Mechanical properties

Nominal stress strain curves of iPP, iPP/Clay, iPP/ESC and iPP/ESC/Clay blends tested at room temperature with cross speed of 5mm/min are presented in figure 1. The tensile parameters of the samples are summarized in table 1.
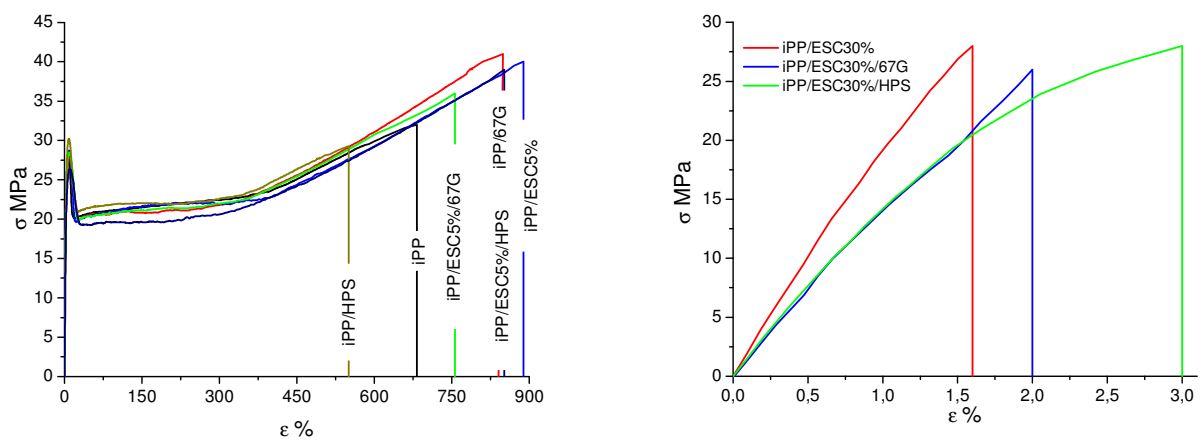
Figure 1: Nominal stress strain curves of iPP, iPP/Clay, iPP/Esc and iPP/ESC/Clay blends

Pure iPP, iPP/Clay, iPP/ESC5% and iPP/ESC5%/Clay exhibit a yield point followed by the necking, cold drawing and fibre rupture, the classic behaviour of semicrystalline polymers at room temperature.

The break parameters for iPP/HPS are lower than that of iPP, whereas iPP/67G presents higher values of σ_b, ε_b. These results are in agreement with morphological analysis by SEM and TEM. In fact iPP/HPS shows many gross domains of clay that contribute to flaw during mechanical stretching, leading to the sample breakage before neat iPP. In iPP/67G, even if there is not intercalation or exfoliation of clay, the good dispersion of clay contributes to enhance the break parameters.

The presence of 5% of Escorez enhances the elongation at break at 890% and the stress at break at 40 MPa respect to pure iPP that shows presents ε_b of 673% and σ_b of 34MPa. The presence of clay into iPP/ESC 5% does not affect significantly the break parameters.

For iPP/Clay, iPP/ESC 5% and iPP/ESC/Clay 5% no variation in the yield parameters are observed.

The samples iPP/ESC30% and iPP/ESC30%/Clay show a brittle behaviour with failure before necking. Their tensile behaviour can be interpreted by considering that the addition of Escorez to iPP changes the physical state amorphous iPP from rubbery to glassy phase, making the system harder. Moreover the presence of small domains (observed on the SEM micrographs) and attributed to Escorez phase can act as defects leading to the sample breakage before necking. These samples present also a Young modulus (E) (table 1) higher than neat iPP. In general E depends on two opposing factors: the overall crystallinity and the physical state of the amorphous phase. The decrease of the overall crystallinity with Escorez content, observed by WAXD results, lowers the Young modulus. The hardening of the amorphous phase due to Escorez molecules that increase the T_g of the system, increases the Young modulus. The second effect is predominant on the first one and the overall balance is an increase of the Young modulus. [1]

6.2 Barrier properties

Table IV reports Oxygen transmission rate and the permeability measured at 23 °C and at relative humidity of 0% for pure iPP, iPP/Clay, iPP/ESC and iPP/ESC/Clay blends. The value of permeability is an average on 3 tests for each composition on compression moulded film with thickness of about 130 μm. In literature many papers report about the decrease of permeability to the gas in dependence on the clay content in the polymer matrix, explained by the tortuous path theory.[2-4]

In this study a small amount of clays used, does not modify the permeability of polymer matrix both in binary and in ternary systems.

The presence of Escorez decreases the permeability proportionally to the Escorez amount used in the blends. The permeability values of a semicrystalline polymer like iPP depend on two factors: the crystallinity fraction and the physicals state of the amorphous phase. The crystalline phase is considered impermeable to gas, so the higher is the crystallinity fraction the lower is the permeability value. The rubbery amorphous phase is more permeable to gas than the glassy amorphous phase, so the harder is the amorphous phase the lower is the permeability value. In the iPP/ESC blends, the presence of ESC decreases the overall crystallinity of material and, at same time, makes more rigid the amorphous phase of iPP. The overall effect is that the second factor is predominant on the first, confirmed by the increase of the T_g.[1]

The addition of clay to iPP/ESC blends does not affect further the permeability.

Table1:Tensile properties: stress and strain at yield (σ_y ε_y), stress and strain at break (σ_b ε_b) and Young's Modulus (E)

Sample	σ_y (MPa)	ε_y %	σ_b (MPa)	ε_b %	E (MPa)
iPP	30±2	7±1	34±4	673±65	1427±13
iPP/67G	28±1	10±1	41±1	849±32	1230±85
iPP/HPS	30±1	8±1	29±2	550±39	1451±81
iPP/ESC5%	29±1	9±1	40±1	889±55	1372±55
iPP/ESC30%	-	-	28±2	2±1	2188±93
iPP/ESC5%/67G	28±1	9±1	36±3	756±84	1408±70
iPP/ESC5%/HPS	26±1	10±1	39±1	851±46	1209±78
iPP/ESC30%/67G	-	-	26±2	2±1	1665±192
iPP/ESC30%/HPS	-	-	28±1	3±1	1672±82

Table 2. Oxygen barrier properties of iPP, iPP/Clay, iPP/ESC and iPP/ESC/Clay blends

Sample	OTR (cm^3 / (24h*m^2))	Permeability (cc*cm/m^2*24h*bar)
iPP	640.8	7.4±0.1
iPP/HPS	417.8	7.3±0.1
iPP/67G	517.6	7.1±0.1
iPP/ESC5%	429.4	5.1±0.1
iPP/ESC30%	331.3	3.3±0.1
iPP/ESC5%/HPS	401.3	5.2±0.1
iPP/ESC5%/67G	428.5	4.6±0.1
iPP/ESC30%/HPS	357.6	3.9±0.1
iPP/ESC30%/67G	266.2	3.2±0.1

References

(1) Silvestre, C.; Cimmino, S.; Duraccio, D. *Focus on Natural and synthetic Polymer Science:* Editor: Cornelia Vasile and G. E. Zaikov, pp.31-47: ISBN l-60021-l l5-l.

(2) Gorrasi, G.; Tortora, M.; Vittoria, V.; Kaempfer, D.; Mülhaupt , R. *Polymer* **2003**, 44, 3679.

(3) Chunsheng, L.; Yiu-Wing M. *Composites Science and Technology* **2007,** 63**,** 2895.

(4) Choudalakis, G.; Gotsis , A. D. *European Polymer Journal* **2009**, 45 , 96

Chapter 7

Rheological Study

In this chapter the rheological properties of iPP, iPP blends and iPP composites are reported. The steady shear viscosity was measured with rotational rheometer and plotted as a function of shear rate for the systems in the range from 190 to 165°C (figures 1, 3, 5 and 6). The shear viscosities are functions of temperature for all samples. In particular the viscosity dropped as the temperature increased. The temperature dependence of the apparent viscosity can be well described by the Arrhenius relation.

$$\ln \eta_a = \ln A + E_a /RT \quad (1)$$

Where A is a material constant, R is the universal gas constant and E is the flow activation energy. The plots of ln ηa versus 1/T at different shear rates for all the compositions are shown in Fig. 2,4,7 and 8. The E_a values at different shear rates are reported in table 1-3. Figure 9 reports the flow activation energy (E_a) calculated at 5s^{-1} as a function of Escorez amount.

In figure 1, shear viscosity of iPP/ESC 5 %and 30% is compared with that of neat iPP. All the samples, at low shear rates (0.01-1 s^{-1}) show Newtonian behaviour, where apparent viscosity η remains at η_0 almost independent of shear rate. However, they show non-Newtonian flow behaviour with marked shear thinning at higher shear rates. [1] The rheology of the iPP/ESC systems show the typical effects of the amount of a low molecular mass component and its dispersion in the iPP. This kind of components (call also plasticizer) are generally small molecules that are chemically similar to the polymer and create gaps between polymer chains for greater mobility and reduced interchain interactions.

Usually, the presence of a plasticizer decreases the viscosity and elasticity of the neat polymer, moreover, the plasticization promotes swelling, enlarging the size of the polymeric domains, and decreasing the specific interfacial area. However, for obtaining such effects the amount of plasticizer has to be enough to ensure interconnectivity of the low molecular phase. [2,3]

The curves reported in figure1 demonstrate that the system iPP/ESC blends shows different behaviour at 5% and 30% in weight. The similar or slightly higher viscosity of the iPP/ESC 5% bend, compared to that of the neat iPP, could be associated with the low amount of ESC that cannot create gaps between polymer chains for greater mobility and reduced interchain interactions. Such morphological feature behaves as a filled polymer system resulting in a slight increase of the viscosity. In other words the small amount of Escorez used (component with small viscosity) is not enough to modify the high viscosity of iPP.

In contrast, the addition of 30% of ESC increases the interconnectivity of this phase, resulting in a rapid percolation of the ESC at this composition range. Thus, the SEM images show a formation of some domains inglobed in polymer matrix, resulting in a significant decrease of viscosity, which is a typical effect of plasticizer.
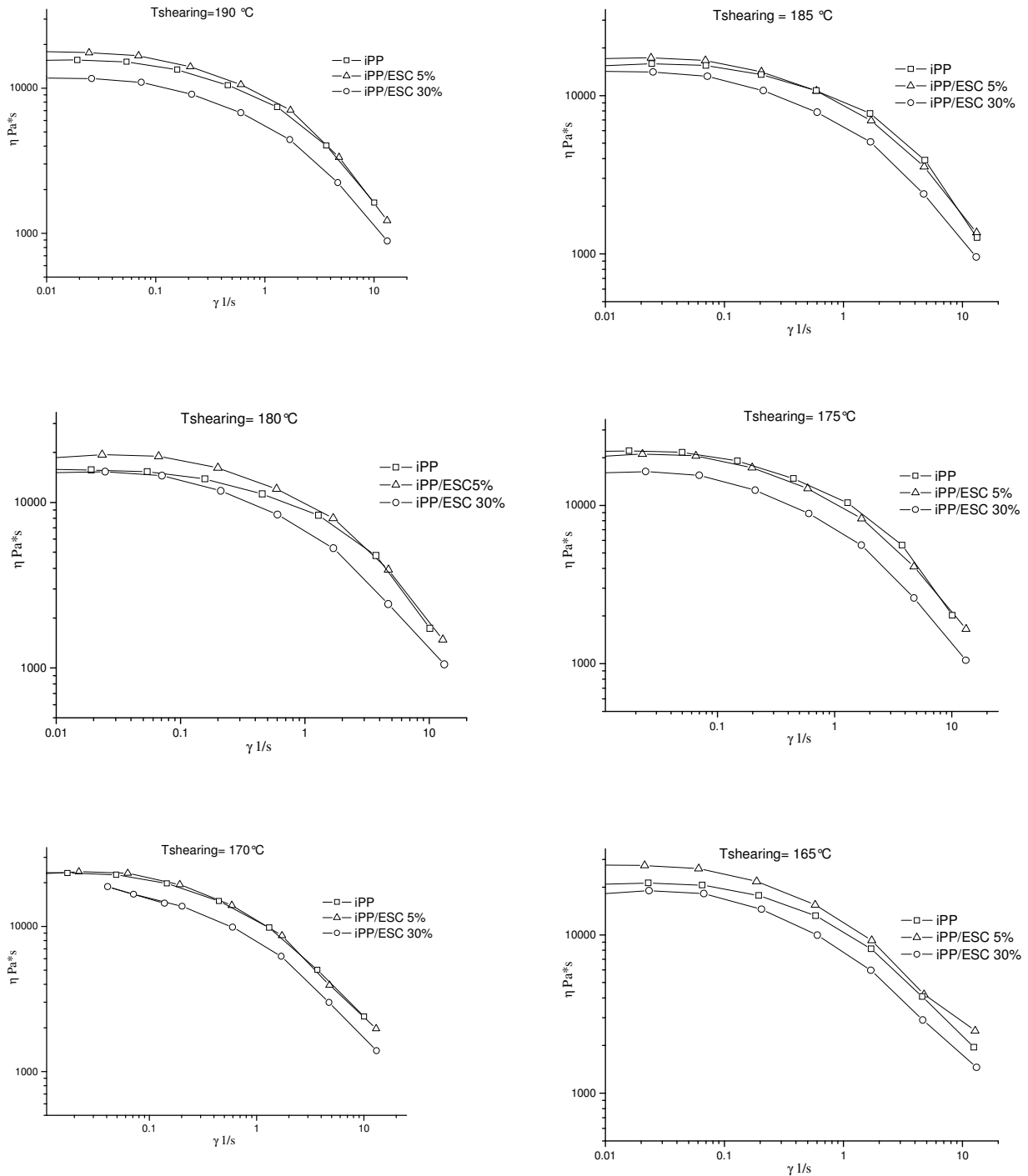
Figure 1: Rheology behaviour for the systems containing 5 and 30 % of Escorez compared with neat iPP at different temperatures.
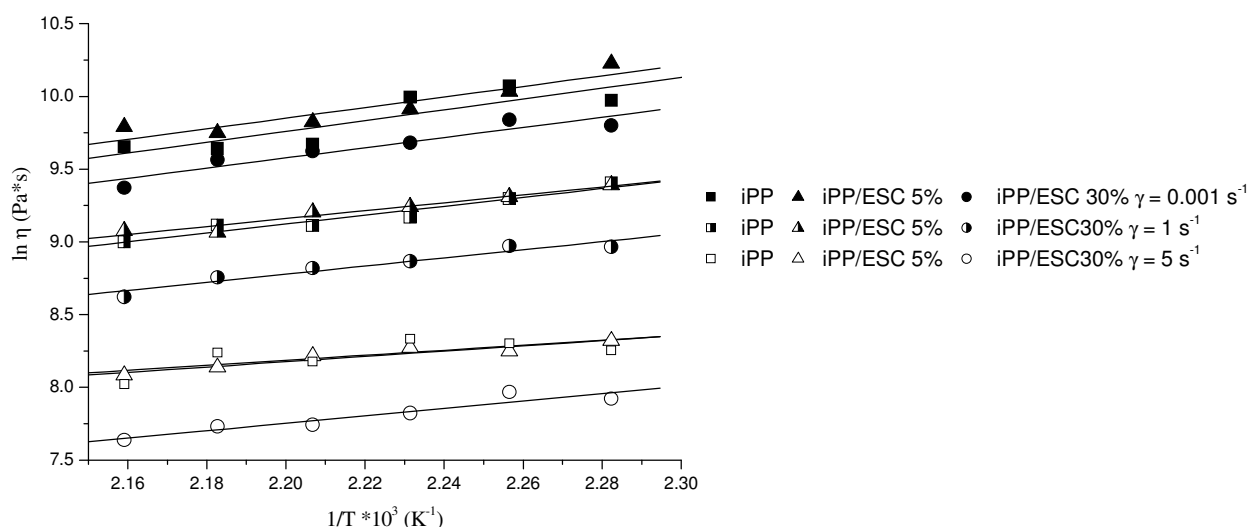
Figure2. Arrhenius plot to determine the flow activation energy of iPP and iPP/ESC blends at constant shear rate

In figure 2, a pretty good linearity for all curves is observed, reflecting that the relationship between $\ln\eta$ and $1/T$ obeys the Arrhenius form (equation (1)). The flow activation energy E_a at a constant shear rate can be determined from the slope of the line by performing the least square fit to the plots. The values of E_a at different shear rate are listed in Table 1. The value of E_a reflects the temperature–sensitivity of the apparent viscosity. The higher the E_a is, the stronger temperature-sensitivity of the apparent viscosity is.

Table 1. Values of E_a of iPP and iPP/ESC at different shear rate								
γ (s^{-1})	0.01			1			5	
	iPP	iPP/ESC5%	iPP/ESC30%	iPP	iPP/ESC5%	iPP/ESC30%	iPP	iPP/ESC5%	iPP/ESC30%
E_a (kJ/mol)	30.9	30.2	29.1	25.4	22.6	23.2	14.3	15.1	21.2

One can observe that for all the series the viscous activation energy E_a reduces with the increase in the shear rate. The melt fluidity of polymer is related to the structure and free volume. The increase in temperature may result in the enhancement of free volume and improvement of chains mobility, and thus may strengthen the melt fluidity and decrease the apparent viscosity. The data in Table 1 indicate that the temperature-sensitivity of apparent viscosity of iPP and iPP/Esc blends become faded with the shear rate. From the table, it can be deduced that no significant change are observed when we increase ESC in the blends.

Figure 3 shows the rheological behaviour for the binary systems iPP/67G and iPP/HPS compares with that of neat iPP.

The composites present the same behaviour of iPP. They display Newtonian plateau (low shear rates) and shear-thinning (at high shear rates) in the same range as the neat polymer. Thus, no significant shear thinning is observed as reported in literature for other kinds of polymer/clay hybrid materials.[4] In the Newtonian region the viscosity for iPP/clay are slightly higher (in particular at 180 and 165°C) or equal to those of iPP. Additionally, viscosities of the composites are comparable with that of pure PP matrix at high shear rates indicating that the shear thinning is dominated by that of pure polymer matrix.
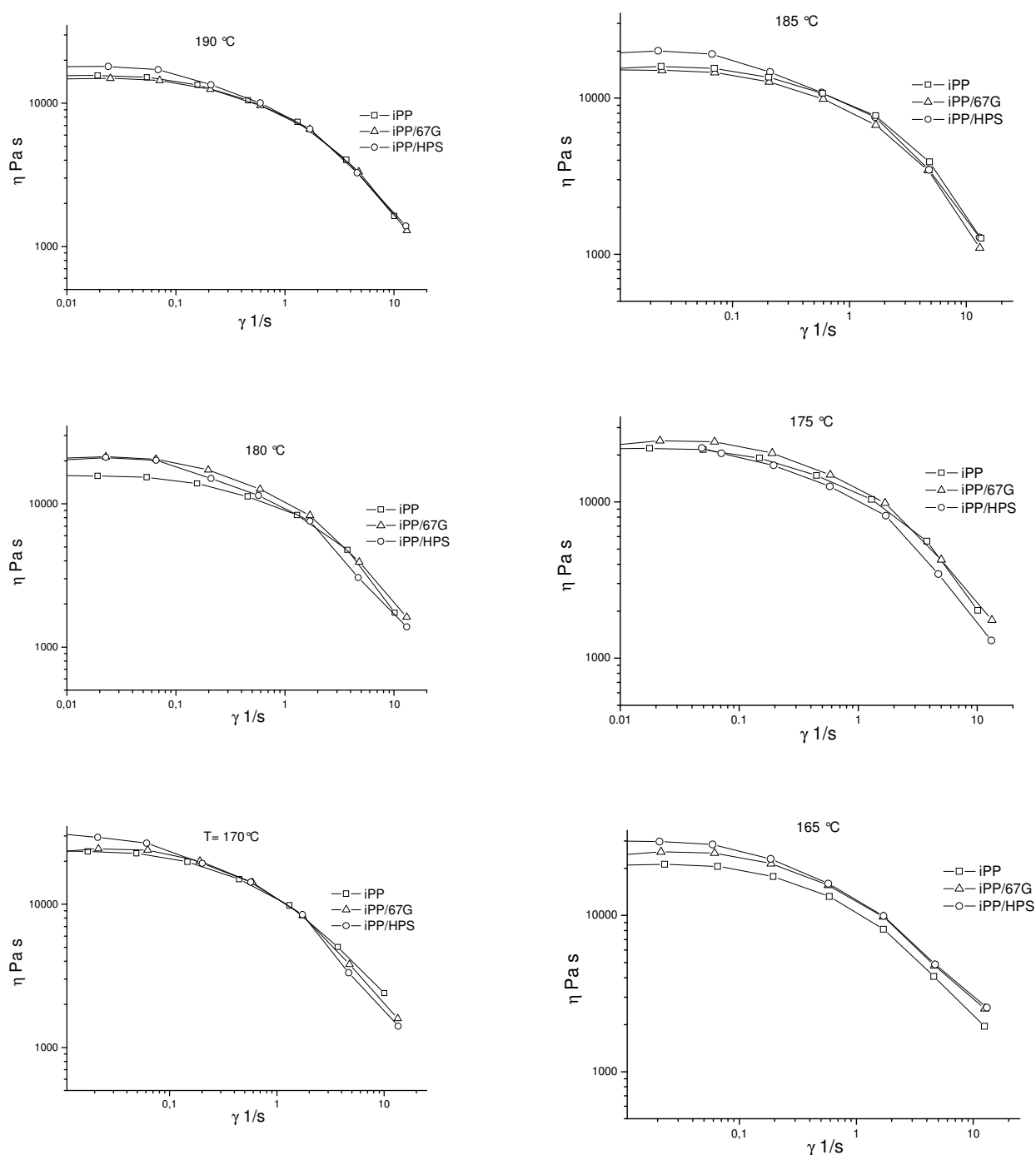
Figure 3: Rheology behaviour for the systems containing iPP/67G and iPP/HPS at different temperatures and for pure iPP.
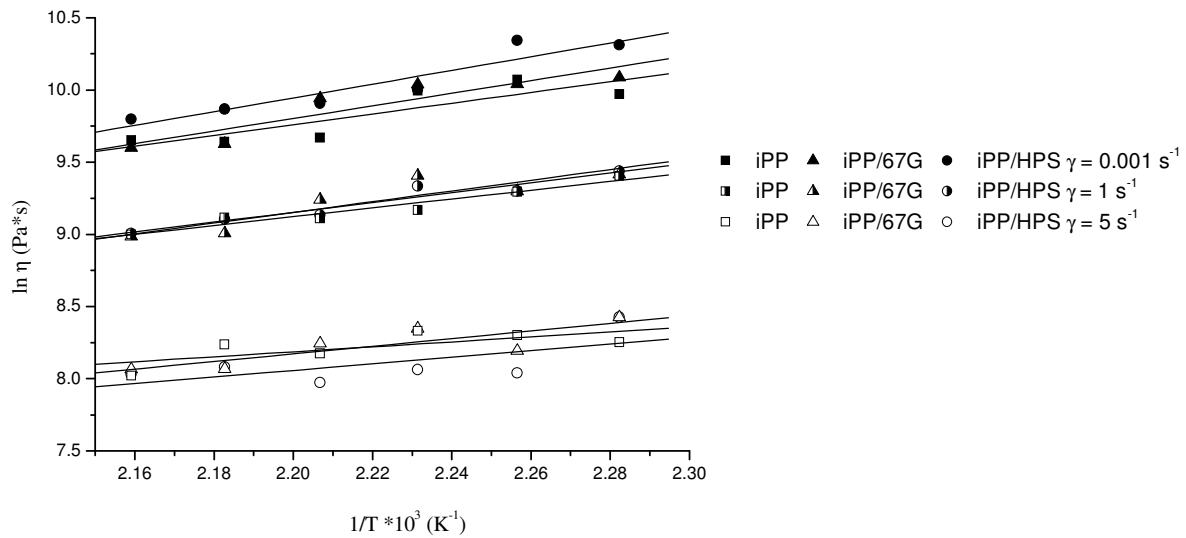
Figure4. Arrhenius plot to determine the flow activation energy of iPP and iPP/clay composites at constant shear rate

From figure 4, it can be deduced that also for these composites a good linearity for all curves is observed, reflecting that the relationship between $\ln\eta$ and $1/T$ obeys the Arrhenius form. As before, the flow activation energy E_a decreases by increasing the shear rate. The E_a value for the composites (table 2) are always higher than that of iPP.

Table 2. Values of E_a of iPP and iPP/clay at different shear rate									
γ (s^{-1})	0.01			1			5		
	iPP	iPP/67G	iPP/HPS	iPP	iPP/67G	iPP/HPS	iPP	iPP/67G	iPP/HPS
E_a (kJ/mol)	30.9	36.6	39.6	25.4	30.7	28.3	14.3	19.0	22.0

Figure 5 and 6 show the rheological behaviour for the ternary systems compared to the binary iPP/ESC5% and iPP/ESC30% respectively. iPP/ESC5%/67G and iPP/ESC30%/67G have the same rheological behaviour of iPP/ESC5% and iPP/ESC30% respectively. iPP/ESC5%/HPS and iPP/ESC30%/HPS present significant decrease in the shear rate steady viscosity in the shear thinning region.
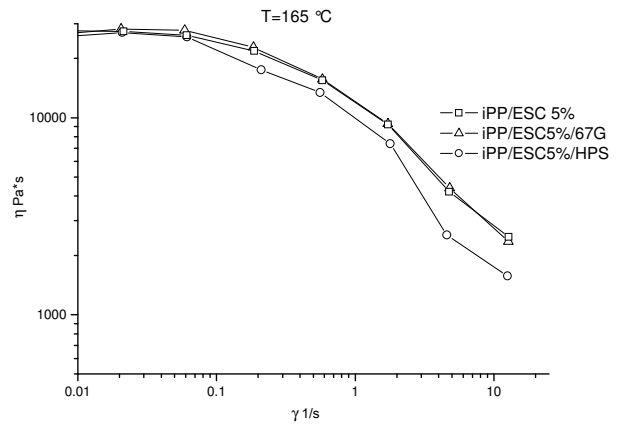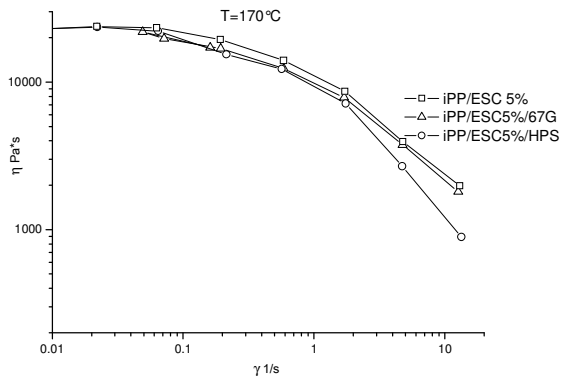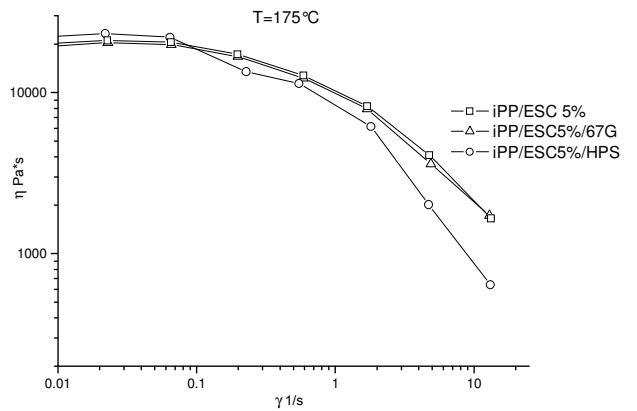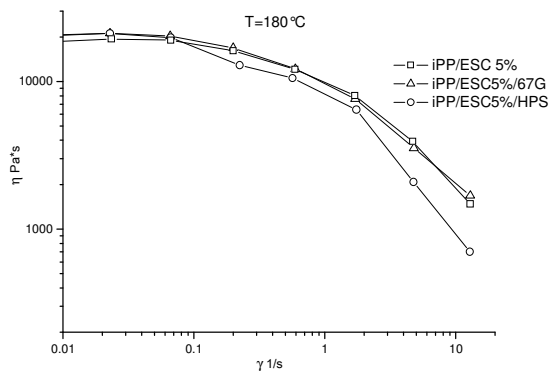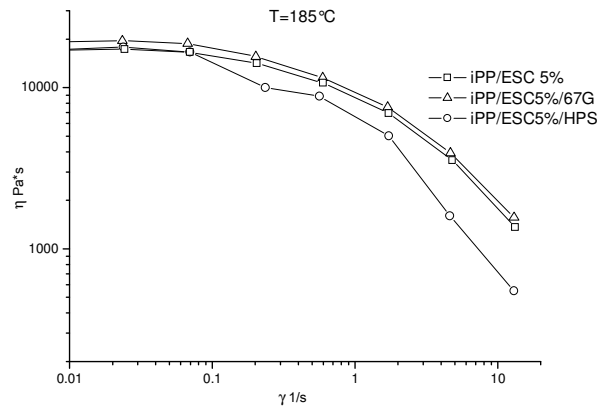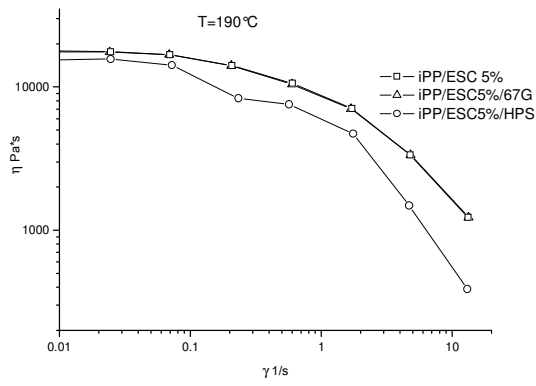
Figure 5: Rheology behaviour for the systems containing iPP/ESC5%/67G and iPP/ESC5%/HPS at different temperatures and for iPP/ESC5%.
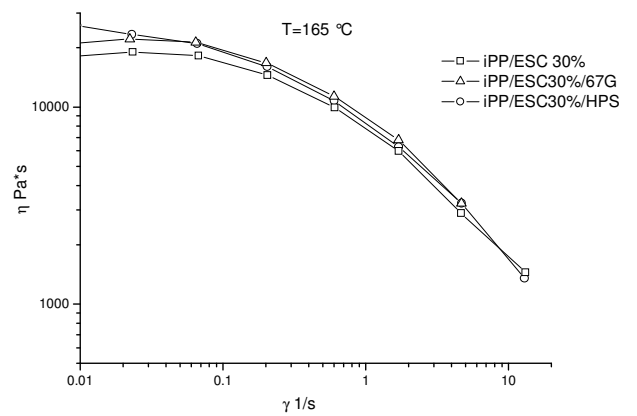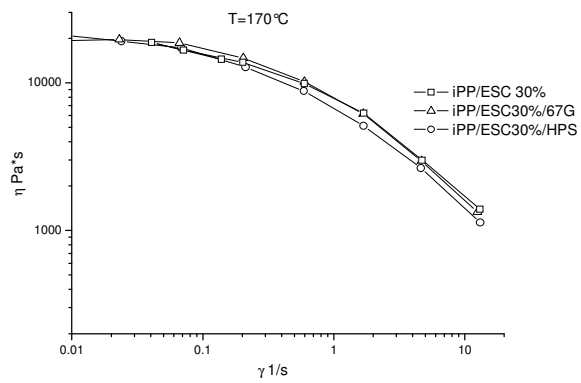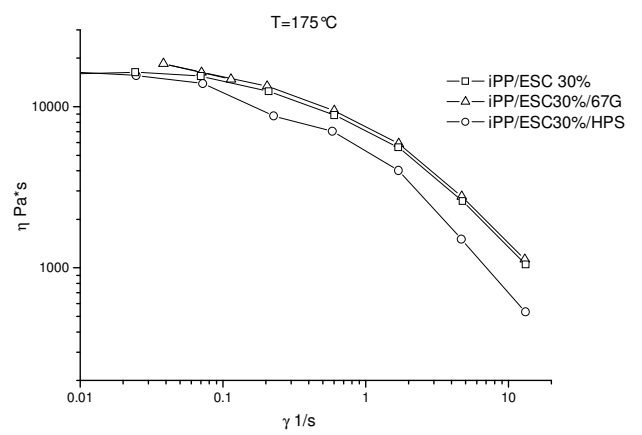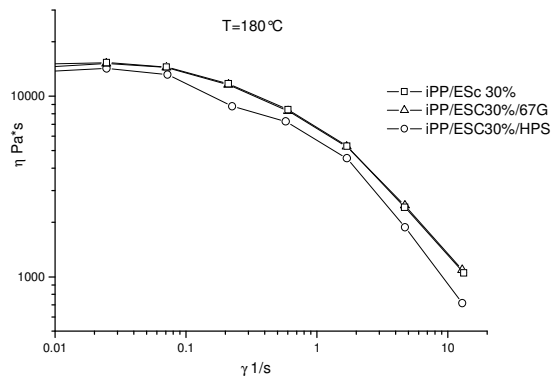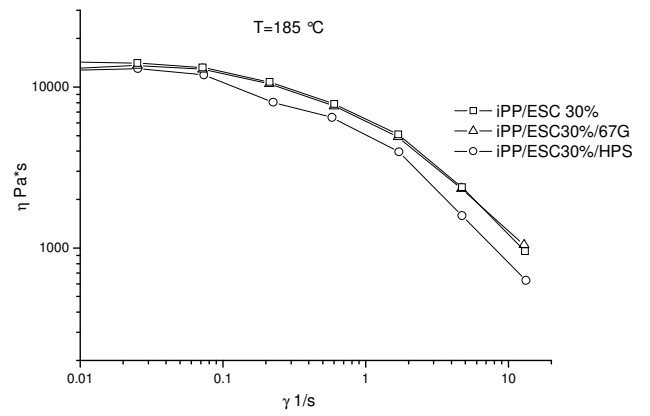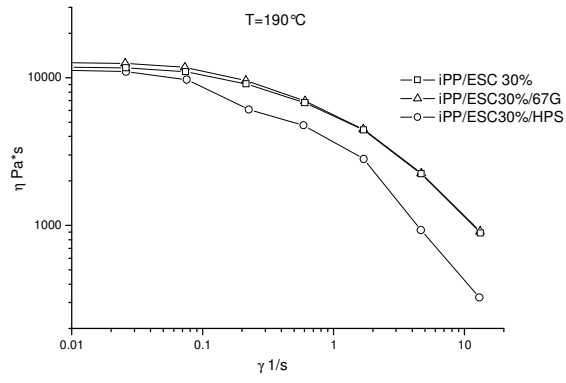
Figure 6: Rheology behaviour for the systems containing iPP/ESC30%/67G and iPP/ESC30%/HPS at different temperatures and for iPP/ESC30%.
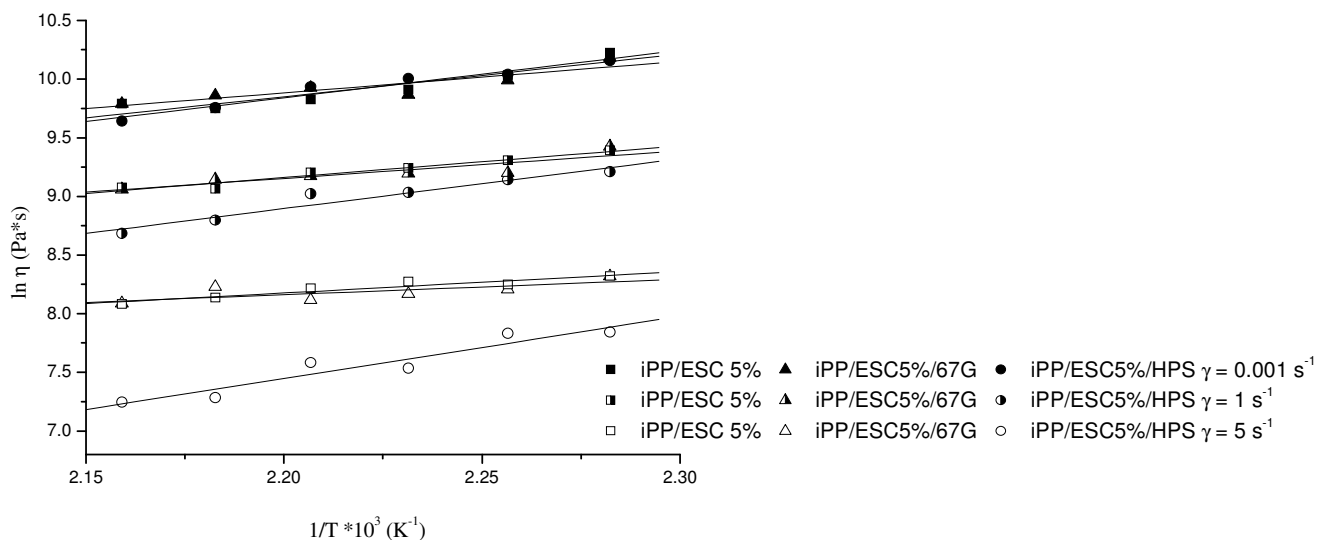
Figure 7. Arrhenius plot to determine the flow activation energy of iPP/ESC 5% and iPP/ESC5%/clay composites at constant shear rate
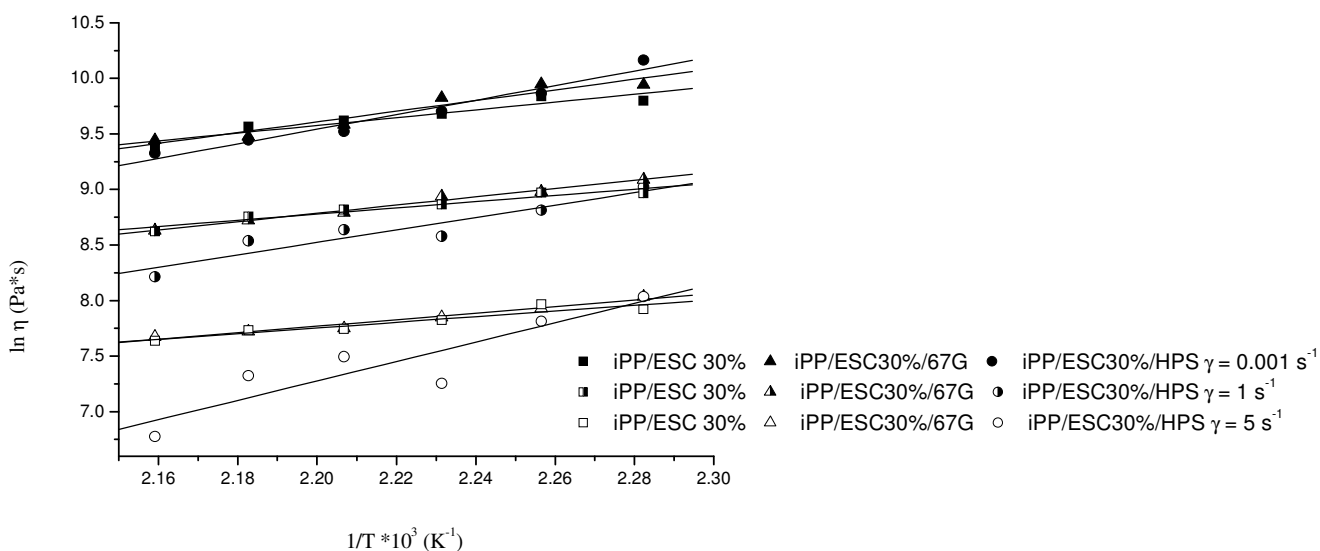
Figure 8. Arrhenius plot to determine the flow activation energy of iPP/ESC 30% and iPP/ESC30%/clay composites at constant shear rate

In figure 7 and 8 the Arrhenius plot for ternary systems containing 5 and 30 % of Escorez respect to iPP/ESC 5 and 30% respectively are reported. The values of the flow activation Energy are reported in table 3. For the samples containing 67G the E_a decreases by increasing the shear rates as for the other samples. iPP/ESC5%/HPS presents an opposite behaviour, with the increase of E_a by increasing the shear rate.

Table 3. Values of E_a of iPP/ESC 5% and 30/ and iPP/ESC5%/Clay and iPP/ESC30%/Clay at different shear rate								
γ (s^{-1})	0.01			1			5		
	iPP/ESC5%	iPP/ESC5%/67G	iPP/ESC5%/HPS	iPP/ESC5%	iPP/ESC5%/67G	iPP/ESC5%/HPS	iPP/ESC5%	iPP/ESC5%/67G	iPP/ESC5%/HPS
E_a (kJ/mol)	30.2	22.2	33.6	22.6	19.5	35.2	15.1	11.1	44.1
	iPP/ESC30%	iPP/ESC30%/67G	iPP/ESC30%/HPS	iPP/ESC30%	iPP/ESC30%/67G	iPP/ESC30%/HPS	iPP/ESC30%	iPP/ESC30%/67G	iPP/ESC30%/HPS
E_a (kJ/mol)	29.1	39.9	54.4	23.2	30.9	54.0	21.2	24.4	72.5

In figure 9 the flow activation energy (E_a) calculated at $5s^{-1}$ is reported as a function of Escorez content for iPP and iPP/clay systems.

It is clearly evident that the systems containing 67 display the same behaviour of iPP by increasing the ESC content. Thus, no significant effect of ESC amount on E is found by considering iPP and iPP/67G. However a different effect is showed by the systems containing HPS. In fact, with 5% of ESC the composite iPP/ESC/HPS shows a significantly increase in the flow activation energy (44.1 kJ/mol) respect to iPP/HPS (22 kJ/mol). The increase is even bigger for the system with 30% of Escorez (72.5 kJ/mol).
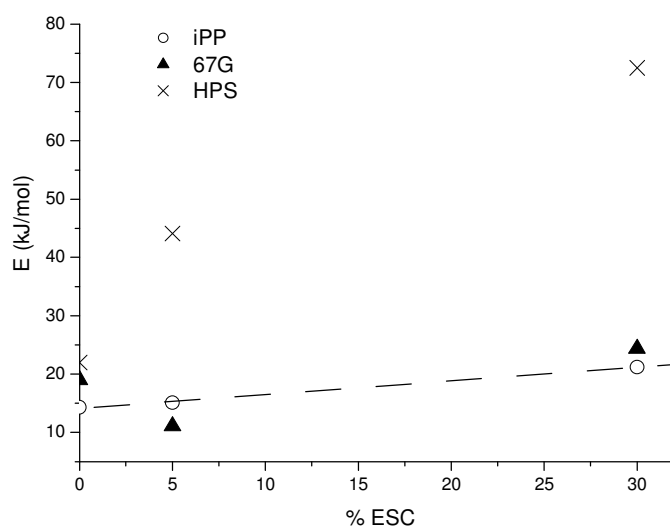
Figure 9: Flow activation Energy (E_a) calculated at 5s^{-1} as a function of Escorez content.

This big effect of the clay HPS on iPP/ESC blends (in particular when the composition is 30%) could be explained with a good swelling of the clay and the oligomer. The clay should have a better affinity for the oligomer respect to iPP and should be dispersed more in this phase respect to iPP. In the low molecular mass phase the clay could orient easily explaining the decrease in the viscosity and the big increase of flow activation energy for iPP/ESC30%/HPS.

References

(1) Yeh Wang, F.B.; Chen, K.C.; Wu, J.C. Wang *Polymer Engineering And Science* **2006,** 46, 289.

(2) Shahbikian S. et al. *Rubber Chem. Technol*. **2011**, 84, 325.

(3) Shahbikian S. et al. *Polymer Engineering & Science*, **2011**, 11, 2314.

(4) Krishnamoorti, R.; Vaia, R. A.; Giannelis, E. P. *Chem. Mater.* **1996**, 8, 1728.

Chapter 8

Crystallization under shear

8.1 Introduction

It is well known that shear flow can significantly change the crystallization kinetics and influence the final morphology of the polymer.[1-3] In particular upon application of the shear, it is possible that some of the polymer molecules in the melt extend in the direction of the flow field and form extended structures. These effects are greatly enhanced in an extensional flow field. It is widely believed that melt flow causes the development of row nuclei in the form of microfibrillar bundles formed from these extended chains,[4-5] which promote the epitaxial growth of folded chain lamellae that filled the space normal (perpendicular) to the row nuclei, resulting in a supermolecular morphological structure known as shish kebab (figure 1). The response of a particular polymeric resin during flow depends greatly on the molecular mass distribution and the associated relaxation spectrum. [6] In particular, the longest chains are the most likely to become extended and form the row nuclei during flow.
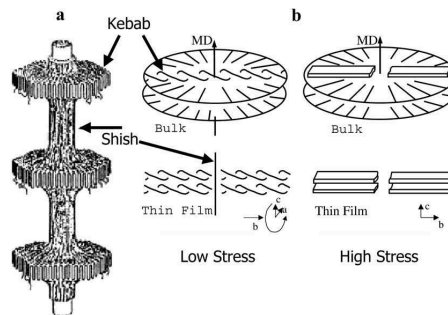
Rajesh H. Somania at al, Polymer 46 (2005) 8587-8623

Figure 1: Morphological structure known as shish kebab

The lamellar crystals which are template by the shish may extend over μm and the shish itself will be much smaller and involve only a very small volume of material. This from an experimental point of view, it may be challenging to physical identify the shish, although the consequences in terms of the common orientation of the 'kebab' is very easily observed.

8.2 Results and discussion

Figures 2 and 3 show selected SAXS patterns (the flow direction is vertical) of iPP after melting at 210°C at different times after applied shear (t=0 s) at 175 and 190 °C respectively.

From Figure 2 it can be seen that an orientated superstructure evolved in the polymer melt after the application of a step shear. The equatorial maxima emerged at about 2 min and resulted from the formation of lamellae layers (or kebab) oriented perpendicular to the flow direction. Further cooling produces the growth of isotropic lamellae that give arise to the scattering ring (image C). As reported in the literature [7] the meridional maxima parallel to the flow direction which arise from the formation of "shish" should appear in the very early stage of crystallization. In the patterns reported here these maxima are hardly detectably. This result could arise from different reasons: i) low concentration of the shish structures at this share rate; ii) shish structures are too small that they are beyond the detection limits of the SAXS setup; iii) as the kebab-like structures grow from the shish, the rodlike scatterer becomes "cylindrical"-like. As this cylinder grows radially, its scattering converges toward the origin and finally disappears [8]. Please note that these patterns were obtained at the SAXS beam line which is not optimised for observing features at very low angles due to the beam collimation and the size and shape of the beam stop which was available.

| t=0 min | t=2 min | t=15 min |
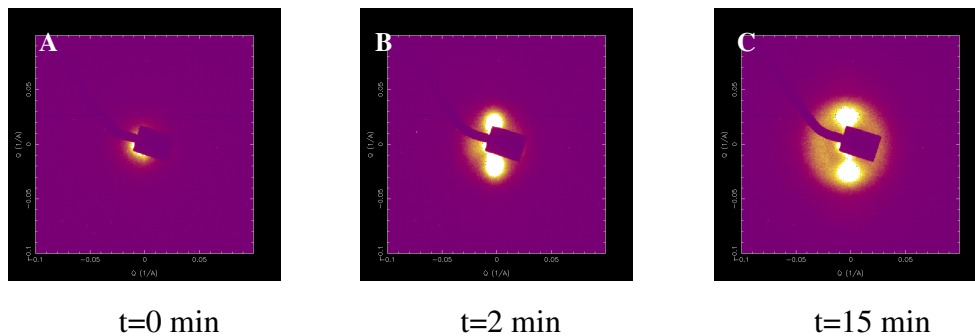
Figure2:2D SAXS patterns of iPP melt at selected times after shear at 175°C

In Figure 3 it is clearly evident from the SAXS pattern that the crystallization process is different from the previuous one shown in Figure 2, in fact, no oriented structure are detectable, indicating that at the point of crystallisation there was no "memory" of shear deformation.

t=0 min   t=5 min   t=15 min
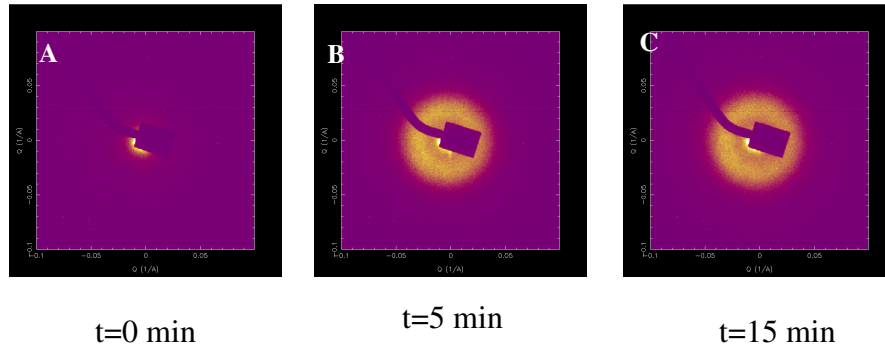
Figure3: 2D SAXS patterns of iPP melt at selected times after shear at 190°C

In terms of the blends studied in this work, the same type of analysis has been carried out. In particular in this chapter, the difference of the shear and temperature profile on the crystallization temperature T_c and on the fraction of oriented polymer crystals (ϕ_{or}^{cryst}) observed will be discussed.

The T_c value is determined from the maximum of the first derivate of invariant (Ω), $d\Omega/dt$. The invariant is calculated from the whole pattern using equation 1.

$$\Omega = \int_{0}^{\pi/2} \int_{Q=0}^{Q_{max}} |\underline{Q}|^2 I(|\underline{Q}|, \alpha) \sin \alpha \, dQ d\alpha \quad \text{Eq.1}$$

The value of the invariant is proportional to the square of the electron density differences in the sample. In the early stages of crystallisation, the value is proportional to the volume fraction of crystals present in the same. However, if there are temperature reduces, the density difference between the crystalline and amorphous phases reduces and the space between lameallae also crystallises and these all serve to reduce the electron density difference and in general the invariant will drop even though the level of crystallinity is slightly increases. If we take the first derivative this is a measure of the growth rate of the fraction of crystallinity and the maximum identifies the temperature at which the sample exhibits the highest growth rate if crystallinity in a similar manner to the peak in the DSC curve during isothermal crystallisation. Figure 4 shows a plot of the invariant and the derivative and the similiarity to the DSC curve becomes apparent.
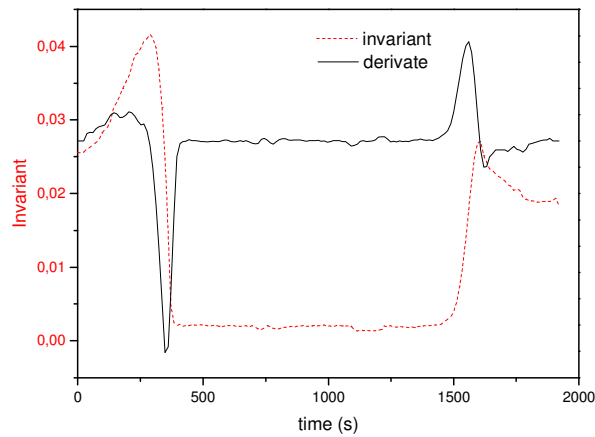
Figure 4: Example of invariant curve and its derivate

In these experiments some of the iPP molecules can crystallise on cooling on row nuclei generated by the shear flow that therefore provides a common axis for crystallisation and an anisotropic distribution of crystals as against crystallisation nucleated by random nuclei.

So in that sense it becomes interesting to separate out the crystal population into that which was directed by a row nuclei and that which was nucleated by random nuclei. In order to estimate the volume of anisotropic crystals from the SAXS patterns, the total intensity was separated into two components: an isotropic component arising from the randomly distributed scatters on the sample and an anisotropic component due to the presence of oriented species.[9-10] The total intensity is therefore represented as:

$$I_{tot}=I_{iso}+I_{or} \qquad \text{Eq.2}$$

The isotropic component is azumutally independent (I_{iso}) whereas the anisotropic contribution exhibits dependence on the azimuthal angle (I_{or}). Such an approach implies that I_{iso} arises only from randomly distributed objects, whereas every oriented scatterer in the sample will contribute to the total intensity only with an isotropic intensity.

The fraction of oriented polymer crystals can be obtained from equation (3):

$$\phi_{or}^{cryst} = \frac{I_{or}(T)}{I_{total}(T)} \qquad \text{Eq. 3.}$$

For the samples containing the clay the fraction of oriented polymer crystals (ϕ_{or}^{cryst}) can be obtained from equation 4:

$$\phi_{or}^{cryst} = \frac{I_{or}(T) - I_{clay}(T)}{I_{total}(T) - I_{clay}(T)} \qquad \text{Eq.4}$$

where T is the temperature at which was applied the shear.

An example of ϕ_{or}^{cryst} vs time, according to equation.4, has been presented in figure 5.
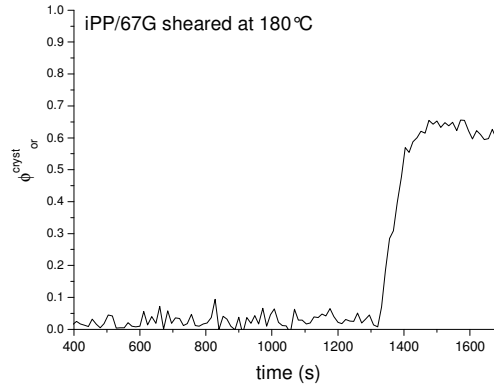
Figure 5: Example of ϕ_{or}^{cryst} vs time

Figure 6 shows the T_c vs T_s (temperature at which was applied the shear) for all the samples. It is clear that the T_c decreases by increasing the T_s.

The level of anisotropy in the SAXS pattern, <P$_2$> was calculated using the following equation 4:

$$< P_2 >_Q = \frac{1}{P_2^m} \int_0^{\pi/2} \frac{I(|\underline{Q}|, \alpha) \sin \alpha P_2(\cos \alpha) d\alpha}{I(|\underline{Q}|, \alpha) \sin \alpha d\alpha} \qquad \text{Eq.4}$$
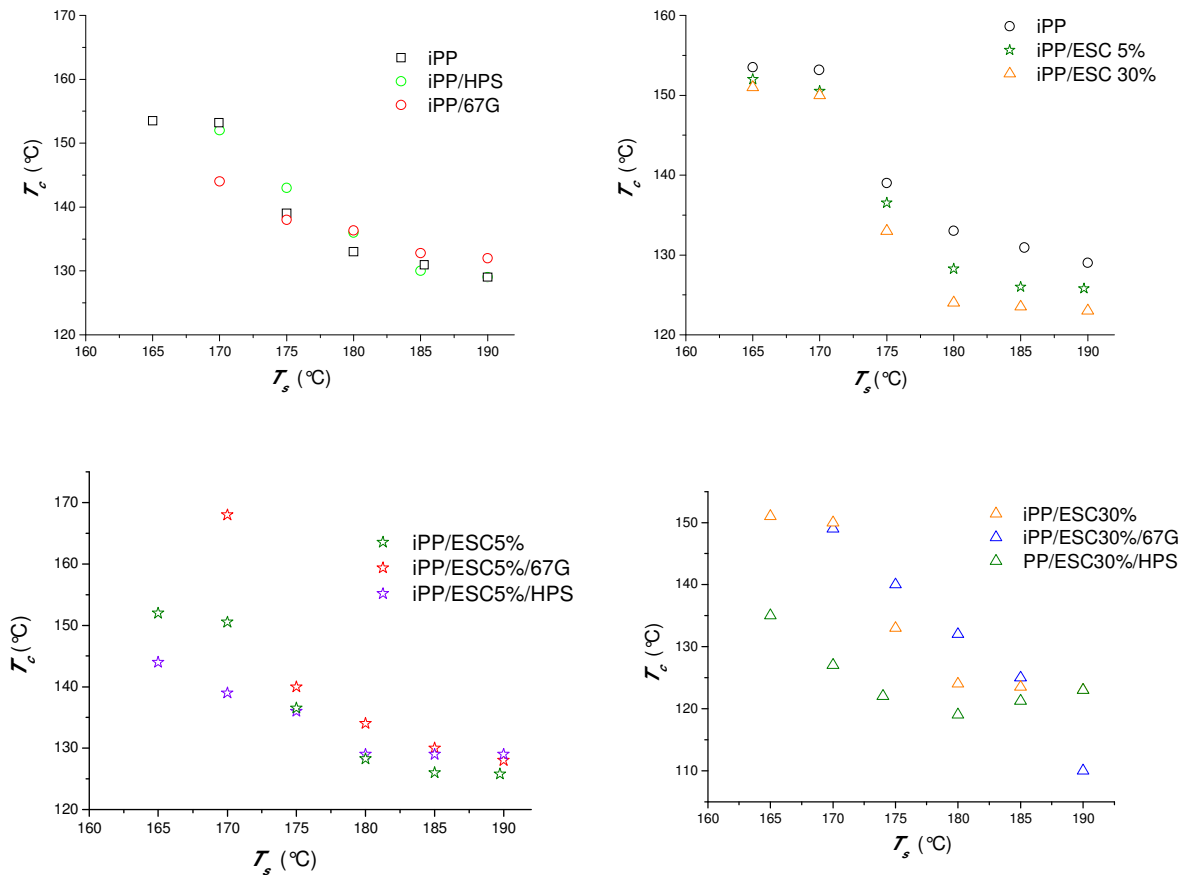
Figure 6: T_c **vs** T_s **for iPP and iPP/Clay, iPP/ESC iPP/ESC/Clay**

Figure 7 indicates that the level of anisotropy increases by decreasing the temperature at which the shear was applied, $T_{s..}$. The differences in the level of anisotropy which develops during crystallization is attributed to the variation in the relaxation processes which take place in the period between cessation of shear flow and the nucleation of crystallization. In these experiments a high value of T_s means that as the sample was cooled at a constant rate, the time period between the shear flow and subsequent crystallisation is probably longer as a consequence of the greater temperature difference. The higher value of ϕ_{or}^{cryst} at low T_s with respect to the value ϕ_{or}^{cryst} at high T_s is due to the reduction of the 'relaxation' period prior to crystallization that was insufficient to allow the conformation of the macromolecules to relax to their equilibrium state prior to crystallisation (figure 6).

The results are now considered in more detail. The presence of both types of clays clearly reduces the ϕ_{or}^{cryst} respect to neat iPP.

The influence of the Escorez ϕ_{or}^{cryst} depends on the Escorez content in the blends. In particular for the blends containing 5% in weight at high shear rate the orientation parameter

77

is higher than that of neat iPP; at low value of shear temperature is lower than that of pure iPP. For iPP/ESC30% blend the level preferred orientation is similar to that of iPP at high shear temperatures, whereas it becomes lower at low shear temperatures.

The presence of HPS in the iPP/ESC blends does not modify ϕ_{or}^{cryst}, whereas the presence of 67G have a different behaviour respect to HPS. In particular in the ternary systems iPP/ESC5%/67G ϕ_{or}^{cryst} is lower than that of iPP/ESC5% only the value at T_s is higher. For the samples iPP/ESC30%/67G the ϕ_{or}^{cryst} value is always higher that the binary blend iPP/ESC30%.
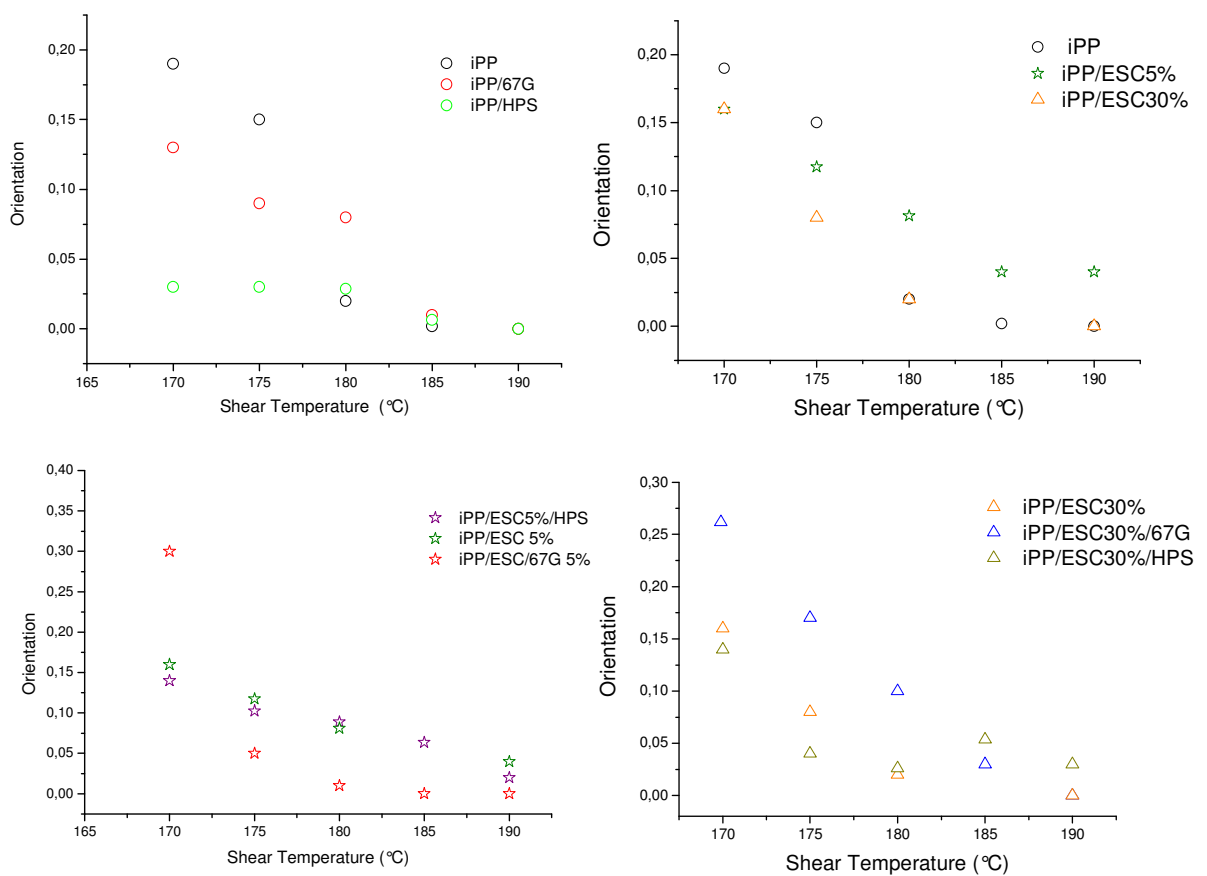
Figure 7: Orientation vs *Ts* for iPP and iPP/Clay iPP/ESC and iPP/ESC/Clay blends

In order to verify if there is the clay directs the crystallisation of iPP playing the part of the extended chains (as the shish) during the formation of the oriented superstructures, a Couette style cell is used in the same basic shear cell that replace the parallel plates (as describe in the experimental chapter). In such an arrangement the scattering vector lies in the plane containing the flow direction and the velocity gradient.

Figure 8 illustrates selected typical SAXS patterns collected at room temperature (A), in the melt (B), during the shear at 170°C (C), at the end of the measure at room temperature in the

normal (D$_1$) and in the edge direction (D$_2$). These patterns clearly show evolution of oriented structures.

Figure 8A shows a well developed isotropic ring typical of the semicristalline polymers prepared by compression molding. At higher Q value a diffuse equatorial streak is present suggesting that preferentially the clay layers are oriented normal to the equatorial direction, ie parallel to the flow direction. This orientation is still present in the melt (figure 8 B) and is due to the particular used method of samples preparation (see experimental part chapter 1). This also confirms that the 67G is well dispersed in the polymer matrix. During the shearing the orientation of the clay is removed as can be seen from figure 8 C. The meridional maxima (due to layer-like oriented structure, or kebab, perpendicular to flow direction) emerges and can be seen at the end of the experiment at room temperature in figure 4 D$_1$.and D$_2$. Again in this figure no clay orientation is present. Moreover as already stated before no meridional reflection are detected in the melt. The possible reasons are the same as before.

It is possible to conclude that 67G does not acts as template for the process of polymer crystallization. iPP melt only retains a memory of the applied shear deformation, which manifest itself through the formation of anisotropic morphology.

The same features are observed in the small angle scattering patterns for iPP/HPS, (figure 9 A-D) with the only difference that before starting experiment and in the melt (Figure 9A and B), clay HPS is not oriented. This could be attributed to the fact that it is not well distributed in the polymer matrix. Again figures 9 D$_1$ and D$_2$ the classical scattering pattern attributed to iPP shish-kebab lamellar structures is present.

A Room Temperature

B melt

C Under shear

D₁ the end of the experiment

D₂   the edge direction at room temperature

Figure 8: SAXS patterns for iPP/67G collected at room temperature (A), in the melt (B), during the shear at 170°C (C) at the end of the experiment (room temperature) in the normal (D₁.) and in the edge direction (D₂).

A Room Temperature

B melt

C Under shear

D₁ the end of the experiment
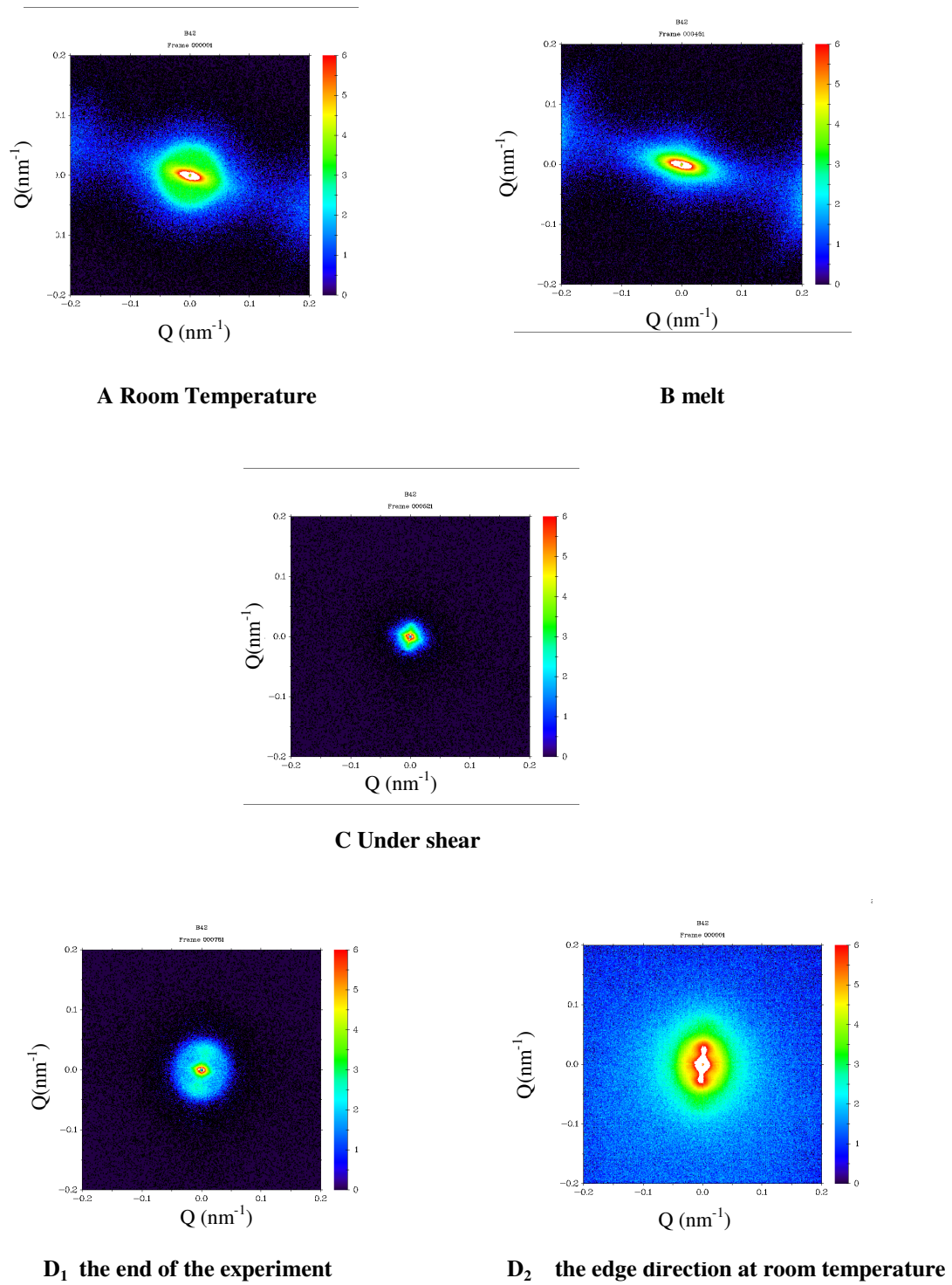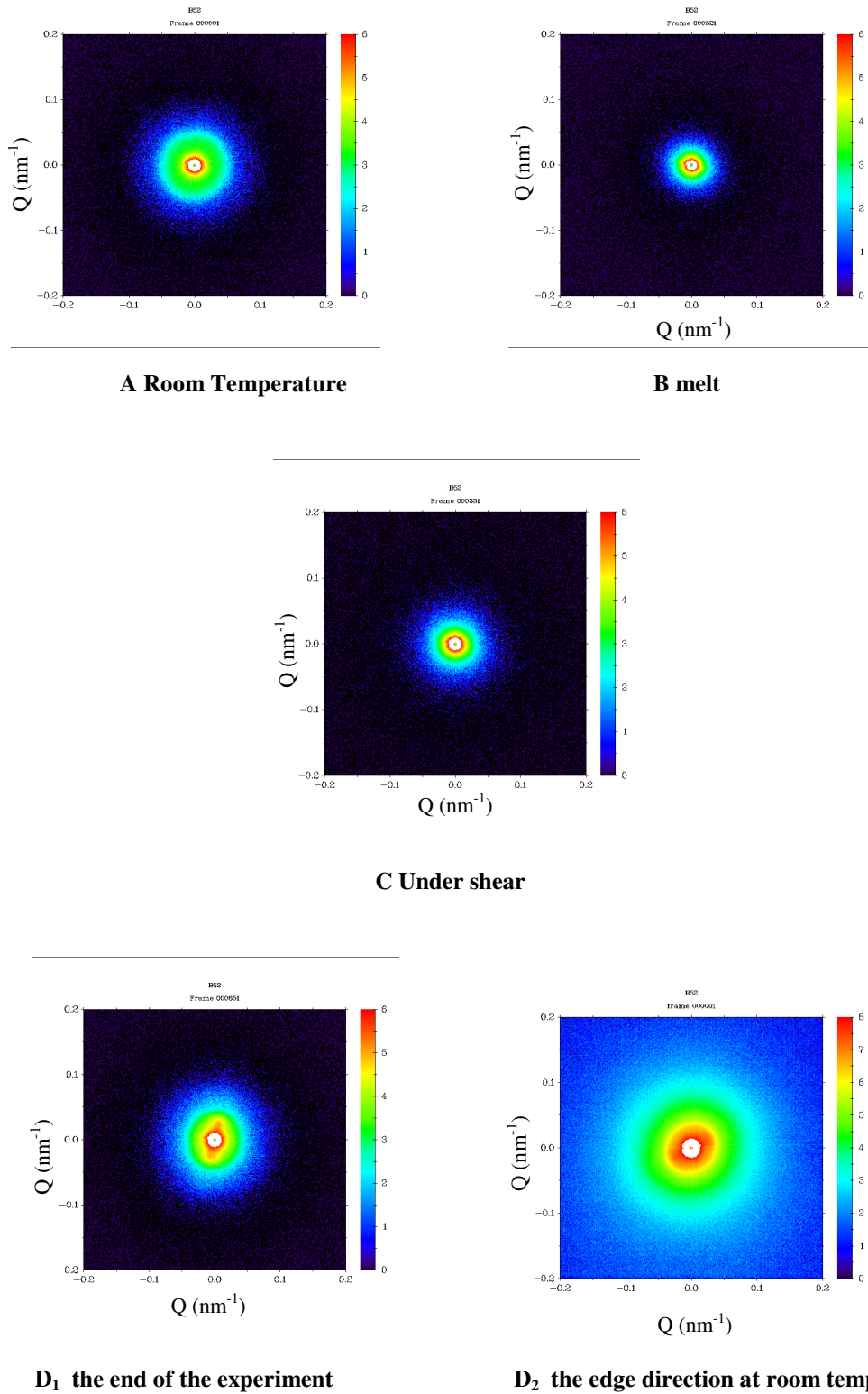
D₂ the edge direction at room temperature

Figure 9: SAXS patterns for iPP/HPS collected at room temperature (A), in the melt (B), during the shear at 170°C (C) at the end of the experiment (room temperature) in the normal (D₁.) and in the edge direction (D₂).

The in-situ SAXS experiments have revealed that the temperature at which crystal growth rate is at a maxima is strongly dependent on the temperature at which the shear flow was applied. In the melt after shear flow, the polymer chains which were extended will be relaxing towards isotropic state. If crystallisation takes place before the chains are full relaxed, the extended chains acts as row nuclei which has 2 consequences. The first is a high level of common orientation of the crystals and second that crystallisation occurs at a higher temperatures, essential the chains are nucleating agents. As the polymer will crystallise in any event, the questions is really how much is directed by row nuclei and how much by randomly arrange nuclei. This changes the crystallisation temperature and the level of anisotropy. The clay platelet orientation is affected by flow but it does not template the crystallisation, although clearly the crystallisation behaviour depends on the details of the clay and other components.

References

(1) Flory, P.J.; *J. Chem Phys.* **1947**,15, 397.

(2) Somani,R.H.; Yang, L.; Hsiao, B.S.; Agarwal, P.K.; Fruitwala, H.A.; Tsou, A.H. *Macromolecules* **2002**, 35, 9096.

(3) Jerschow, P.; Janeschitz-kriegl, H. *Int. Polym.Process.* **1997**, 12, 72.

(4) Eder, G.; Janeschitz-Kriegel, H.; Liedauer, S.; *Prog.Polym. Sci*. **1990**, 15, 629

(5) Kumaraswamy, G.; Issaian, A.M.; Kornfield, J.A.; *Macromolecules* **1999**, 32, 7537

(6) Pople, J. A.; Mitchell, G. R.; Sutton, S. J.; Vaughan, A. S.;. Chai, C. K.; *Polymer* **1999**, 40, 2769.

(7) Somani, R. H.; Hsiao, B.S.; Agarwal, P.; Fruitwala, H.; Tsou, A.H. *Macromolecules* **2002**; 35, 9096

(8) Schultz, J.M.; Hsiao, B.S.; Samon J.M. *Polymer* **200**0, 41, 8887

(9) Somani, R.H.; Hsiao, B.S.; Nogales, A.; Srinivas, S.; Tsou, A.H.; Sics, I. et al. *Macromolecules* **2000**; 33, 9385

(10) Nogales, A.; Hsiao, B.S.; Somani, R.H.; Srinivas, S.; Tsou, A.H.; Balta-Calleja, F.J. et al.; *Polymer,* **2001***;* 42, 5247

Conclusions

This thesis aimed at completing the study of the properties of iPP modified with an hydrogenated oligomer resin and at improving these properties by making nanocomposites with the addition of clays for possible use in the food packaging sector.

All the binary and ternary blends have been prepared by melt mixing and the processability conditions (temperature, time and speed of mixing) have been optimized. The systems were characterized by rheological, morphological and structural analysis. Calorimetric, thermogravimetric and mechanical and barrier characterization was also carried out.

From the results obtained the following conclusions can be draw:

1. The iPP is not intercalated between clay layers. On the other side a discrete dispersion of the 67G in the matrix (iPP and iPP/ESC blends) is observed, whereas unmodified clay (HPS) forms large agglomerates.

   For the binary and ternary systems containing 5% of Escorez an homogenous fractured surface is observed whereas for the system iPP/ESC30% small domains of Escorez are detected, indicating a phase separation between iPP and Escorez in amorphous phase.

2. The glass transition temperature, T_g, values of iPP/HPS and iPP/67G composite are similar to that of plain iPP. For the binary and ternary systems containing 5% of Escorez the T_g increases of 8-11°C (see table 1 in chapter 4) confirming the compatibility between iPP and Escorez in amorphous phase, according to the morphological results and literature data. For the iPP/ESC and iPP/ESC/Clays blends containing 30% of Escorez, (where according to literature phase separated melts should be obtained), a single T_g with values higher respect that of iPP is observed . The transition of ESC domains visible by SEM (expected to be in the range 80-90°C) is not detectable because probably the amount of this phase is too small and behind the DSC sensibility.

3. In air atmosphere the addition of clay (both HPS and 67G) slightly increases the thermal stability of iPP. This small increase is probably due to a physical barrier effect of the silicate layers. The samples containing ESC (5 and 30%) show a significant increase of thermal stability in air in terms of T_{10} and T_{mr} temperatures compared to the pure iPP. The increase is proportional to the amount of Escorez. It is possible that Escorez acts as a stabilizer for iPP binary and ternary systems by retarding the autocatalytic propagation of carbon radicals. The addition of clay to iPP/ESC blends does not further affect the thermal stability of these blends. In nitrogen atmosphere a small decrease of T_{10} and T_{mr} is observed for 67G whereas unmodified clay (HPS) does not affect the thermal stability of iPP. For all the other samples no significant differences are detectable respect to neat iPP in inert condition.

4. The presence of both clays in iPP/Clay systems does not modify the rheological behaviour of neat iPP. The rheological behaviour of iPP/ESC blends is depending on composition. For the iPP/ESC 5% blend a very slight increase in the higher viscosity is observed. This low amount of Escorez is not enough to modify the high viscosity of iPP. Increasing the amount of Escorez the interconnectivity of this phase increased, resulting in a rapid percolation of the ESC at this composition range.

   No variations of E_a is found for iPP/ESC5%/67G iPP/ESC30%/67G respect to iPP/67G. A big effect is found with clay HPS in iPP/ESC blends (in particular when the composition is 30%). This could be explained with a good swelling of the clay and the oligomer. HPS should have a better affinity for the oligomer respect to iPP and should be dispersed more in this phase respect to iPP

5. iPP, iPP/Clay, iPP/ESC5% and iPP/ESC5%/Clay exhibit the classic behaviour of semicrystalline polymers at room temperature. The parameters at break for iPP/HPS are lower than those of iPP, whereas iPP/67G presents higher value of σ_b, ε_b. These results are in agreement with morphological analysis by SEM and TEM. The samples iPP/ESC30% and iPP/ESC30%Clay show a brittle behaviour with failure before necking: the addition of Escorez to iPP changes the physical state amorphous iPP from rubbery to glassy phase, making the system harder. Moreover the presence of small domains (observed on the SEM micrographs) and attributed to Escorez phase can act as defects leading to the sample breakage before necking.

6. The permeability of iPP decreases proportionality with the amount of the Escorez in the blend and the presence of the clay both in binary and ternary systems does not modify the permeability.

7. The non isothermal crystallization behaviour in quiescent conditions depends on composition and cooling rate. Both the increase of cooling rate and the addition of clay and/or ESC shifts the crystallization onset to lower values indicating that the nucleation process occurs at lower temperature. These results can be attributed to the diluent effect of ESC (for the binary and ternary blends containing ESC) and to the presence of clay particles that effect the transport of macromolecules chains toward the growing nuclei.

8. The in-situ SAXS experiments have revealed that the temperature at which crystal growth rate is at a maxima is strongly dependent on the temperature at which the shear flow was applied. In the melt after shear flow, the polymer chains which were extended will be relaxing towards isotropic state. If crystallisation takes place before the chains are full relaxed, the extended chains acts as row nuclei which has 2 consequences. The first is a high

level of common orientation of the crystals and second that crystallisation occurs at a higher temperatures, essential the chains are nucleating agents. As the polymer will crystallise in any event, the questions is really how much is directed by row nuclei and how much by randomly arrange nuclei. This changes the crystallisation temperature and the level of anisotropy. The clay platelet orientation is affected by flow but it does not template the crystallisation, although clearly the crystallisation behaviour depends on the details of the clay and other components.

At the end of this study it is possible to conclude that two systems can be selected for further investigation: iPP/ESC5%/67G and iPP/ESC30%/HPS.

The iPP/ESC5%/67G presents similar mechanical properties to iPP and improved barrier properties respect to iPP, it could be a good starting point for investigations in order to use the ternary systems in the food packaging. For these systems the improvement of dispersion of the clay nanoparticles must be achieved by optimizing the preparation conditions and the mixing procedures. These improvements surely will bring a substantial further increase of the barrier properties and of the thermal stability and will make these systems very attractive for extensive applications.

For the systems iPP/ESC30%/HPS the result obtained from rheological behaviour suggests further investigations: this system seems to have a better affinity with the apolar Escorez respect to iPP. At this point the modality of blending seems become very important. A masterbach made of Escorez and HPS could present structure intercalated/exfoliated. The addition of this masterbach to iPP due to the possible interactions of iPP with Escorez, in this case present in the layers could bring interesting morphology and possibility to design new nanomaterials with improved properties.